Radboud University Nijmegen

Faculty of Science

Black hole shadows

Shining light on black holes and their mimickers

Thesis BSc Physics and Astronomy

Author:
Mariska Rood

Supervisor:
dr. Béatrice Bonga

Second reader:
dr. Monika Moscibrodzka

July 2020

Abstract

The picture of a black hole made in 2019 tells a lot about the structure of spacetime in a regime in which gravity is strong. By comparing observations with theoretical predictions, such a picture can help finding the ultimate theory of gravity. One way of doing this is by looking at photon paths around different types of black holes. In this thesis, we describe a framework that can be used to predict photon paths around many different types of black holes and black hole mimickers. In addition to studying photon paths, we have also looked at certain properties of the black holes and the photon paths around them. We plotted these photon paths and their properties to gain insight into the behavior of photons around various black holes and their mimickers. This framework can be used during the analysis of observational data from compact objects. In this thesis, we apply this framework to Schwarzschild and Reissner-Nordström black holes in general relativity as well as to boson stars in Einstein-scalar theory.

Contents

1 Introduction

1.1 Discovery of the Black hole solution

General relativity is the most well understood and most well known theory of gravity. It came into the world in 1915, written by Albert Einstein. This theory of gravity changed the perspective on space. It described gravity as a geometric property of not only space, but also time. General relativity is focused around the Einstein equation, that relates the geometric curvature of spacetime to matter. A year after Einstein published his gravitational theory, Karl Schwarzschild discovered the Schwarzschild solution to the Einstein equation. The Schwarzschild solution describes the gravitational field in a vacuum around a spherically symmetric mass. It assumes that the charge and angular momentum of the central object is zero and that the cosmological constant vanishes. The Schwarzschild black hole, which is the name of the black hole that arises from the Schwarzschild metric, is a static solution to the Einstein equation, meaning that the gravitational field around the mass does not change in time. A Schwarzschild black hole can only be distinguished from another Schwarzschild black hole by its mass. Because the angular momentum of a Schwarzschild black hole is zero, there is spherical symmetry in the system. Therefore the spacetime metric only depends on the distance to the mass and not on time or any angles.

Shortly after the discovery of the Schwarzschild solution to the Einstein equation, the Reissner–Nordström solution was discovered. The Reissner–Nordström metric is an extension of the Schwarzschild solution. In this case, the gravitational field does not only depend on the mass, but also on the charge of the object. The Reissner–Nordström metric is, just like the Schwarzschild metric, a static and spherically symmetric black hole solution.

An even more general solution of the Einstein equation is the Kerr solution. This solution is found in 1963 and describes the gravitational field around a rotating object. As a consequence, the Kerr metric is no longer spherically symmetric. The extension of the Kerr solution for charged black holes is called the Kerr-Newman solution. However, in this thesis we will only focus on spherically symmetric black hole solutions. Therefore we will not take a look at the Kerr and Kerr-Newman black hole solutions.

1.2 Astrophysical evidence for black holes

Even though the black hole solution of the Einstein equation has been known for quite some time, it took longer to actually identify such an object in space. For a long time there even was controversy whether or not the idea of black holes was relevant for real-world physics. The following quote by the prominent Nobel prize winning astrophysicist Subrahmanyan Chandrasekhar [1] after the discovery of real-world black holes captures this spirit well:

> *"In my entire scientific life, extending over forty-five years, the most shattering experience has been the realization that an exact solution of Ein-*

stein's equations of general relativity, discovered by the New Zealand mathematician Roy Kerr, provides the absolute exact representation of untold numbers of massive black holes that populate the universe. This "shuddering before the beautiful," this incredible fact that a discovery motivated by a search after the beautiful in mathematics should find its exact replica in Nature, persuades me to say that beauty is that to which the human mind responds at its deepest and most profound level".

Right now there are multiple indirect and direct ways to look for black holes. An example of an indirect way of searching for a black hole is by looking at orbiting stars around a massive object. Based on observations of the velocities of stars orbiting the massive object in the centre of our Milky Way, researchers found that this central object has a mass of around 4 million times that of the sun in a radius of less than half an astronomical unit. The mass in combination with the small radius suggests that we are dealing with a black hole. With these kinds of indirect ways to measure black holes, we predict that there should be millions of black holes in the Milky Way alone and that there should be a supermassive black hole in the centre of each galaxy. However, it is very difficult to study black holes in more direct ways. This has to do with the fact that black holes do not radiate any light.

There has been a boost in observing black holes since 2016. In this year, the LIGO and Virgo detectors measured gravitational waves for the first time. Gravitational waves are another solution of the Einstein equation. As a consequence, measuring these gravitational waves was a huge step in testing general relativity. Many of the gravitational waves detected by LIGO and Virgo were emitted by black holes and thus find their origin very close to the black hole. Therefore they are a better probe of the strong field regime around the black hole than, for example, the stars orbiting the black hole, since their distance to the black hole is much larger. The first detected gravitational waves were coming from a binary black hole merger. This means that in 2016 gravitational waves were added to the list of indirect ways to detect black holes, making it even more probable that black holes really exist.

After the detection of gravitational waves, we did not have to wait long for the direct imaging of black holes. In April 2019 the first ever picture of a black hole was taken by the Event Horizon Telescope [2]. This was the finishing touch in the search for black holes, which started more than a century earlier. Besides providing evidence for the existence of black holes, this black hole picture is also very valuable in testing general relativity and other gravitational theories in the strong field regime.

1.3 Theoretical and observational reasons to look beyond

General relativity has been discovered in 1915 and it endured every test ever since. Among its predictions are gravitational waves, gravitational lensing and black holes. All of which turned out to be true. However this does not mean that it is the ultimate gravitational theory. General relativity is very good at describing the curvature of spacetime under certain circumstances, but it fails to work under extreme conditions

such as at the center of black holes where singularities develop. Moreover, general relativity is not compatible with quantum theory.

Besides general relativity there are also modified and alternative gravitational theories. These theories try to reconcile general relativity with the quantum world, aim to explain the origins of dark matter and dark energy, or aim to improve our understanding of nature in some other ways. It is difficult to test these alternative gravitational theories when there are not that many high regime places in spacetime that visualize the effects of gravity. The two latest discoveries, those of gravitational waves and the direct imaging of black holes, make it easier to compare general relativity with alternative and modified gravitational theories. Especially the direct imaging of black holes is crucial for the research done in this thesis. This is because we compare the image of black holes with the image of black hole mimickers, which exist in modified gravitational theories.

1.4 Null geodesics as probes of physics near these compact objects

In the picture of the black hole you can see photons coming from the black hole. By predicting how these photons act around certain types of black holes and black hole mimickers, it is possible to compare the calculated photon paths with a picture of a black hole. We can predict how photons act around a black hole by calculating the null geodesics of the system. Null geodesics are the paths taken by light rays in the geometric optics approximation, which states that photons follow a straight line in flat space and the shortest path in a curved spacetime. By photons we mean light particles in the classical way. We also looked at massive particles, which follow the time-like geodesics of the system.

In this thesis we make use of some assumptions. One of these assumptions is that the light is coming from right behind the black hole. This is not the case for, for example, the black hole picture. In this picture the photons are coming from the accretion disc around the black hole. Another assumption we make is that the black hole has no angular momentum (and thus is spherically symmetric). This is also not the case for most black holes. Therefore the work in this thesis is a theoretical approach to photon paths and can not be directly related to real-world observations such as the black hole picture.

2 Spherically symmetric systems

In this chapter we will derive the equations of motion and other properties of null geodesics for spherically symmetric spacetimes. We will also look at certain properties for time-like geodesics. In later chapters we will apply the results of this chapter to the spherically symmetric black hole solutions in general relativity as well as to a specific black hole mimicker in a modified gravitational theory. This allows us to calculate photon paths around different types of black holes and black hole mimickers.

2.1 Equations of motion

To calculate the equations of motion it is necessary to define a metric which describes the spacetime we are working with. We define

$$ds^2 = -A(r)c^2dt^2 + B(r)dr^2 + r^2d\theta + r^2\sin^2\theta d\phi^2. \tag{2.1.1}$$

However, in the remaining part of this thesis we write $c = 1$. This metric describes any spherically symmetric and static spacetime. As a result, the metric components only depend on the coordinate r and are independent of time and angles. When applied to spacetimes describing a central object, the component functions A and B can depend on constant properties of the centered object, such as the mass and charge of the object. The metric can be generalized even more by multiplying the angular part by a function that depends on r, which we can call $C(r)$. However, in this case it is possible to rescale Eq. (2.1.1) such that this extra function disappears. Therefore Eq. (2.1.1) already includes this case. The defined metric does not contain any cross-terms.

A metric that is independent on one or more of the coordinates in the system, typically has one or multiple Killing vectors. A Killing vector preserves the metric, that is, it describes the symmetries of the metric. In this case, the metric has time translation symmetry and spherical symmetry. Such a Killing vector gives rise to a conserved quantity along geodesics, which can be described by

$$K_\mu\dot{x}^\mu = \text{constant}. \tag{2.1.2}$$

In this equation $\dot{x}^\mu = \frac{dx^\mu}{d\lambda}$, which we will use for the remainder of this thesis. This quantity is the tangent vector along a geodesic parametrized by λ. The Killing vectors associated with the time translation and spherical symmetry are given by

$$K_\mu = (-A(r), 0, 0, 0) \tag{2.1.3}$$

and

$$K_\mu = (0, 0, 0, r^2\sin^2\theta), \tag{2.1.4}$$

respectively. We will first take a look at Eq. (2.1.3). When we combine this equation with the metric of Eq. (2.1.1), we find

$$A(r)\dot{t} = \text{constant} = E. \tag{2.1.5}$$

This conserved quantity is also called the total energy E of the system, meaning that a symmetry in time translation corresponds to conservation of energy. For Eq. (2.1.4), there is a $\sin\theta$ term. Because we are working with a spherical symmetric system, it is possible to set θ to any constant term. We choose $\sin\theta = \pi/2$, causing the $\sin\theta$ to disappear. When we combine this quantity with the metric in Eq. (2.1.1) we get

$$r^2\dot{\phi} = \text{constant} = L. \tag{2.1.6}$$

This conserved quantity can be called the angular momentum L, so spherical symmetry corresponds to the conservation of angular momentum. There is another constant along the geodesics, which is metric compatibility. One can show that the norm of the tangent vector to the geodesic is also conserved. In particular, we have

$$\epsilon = -g_{\mu\nu}\dot{x}^\nu\dot{x}^\mu. \tag{2.1.7}$$

In this equation, ϵ always has a value of zero for null geodesics. For time-like geodesics (massive particles) ϵ is always equal to 1 and for space-like geodesics ϵ is equal to -1. Specifying this quantity for the chosen metric gives

$$-\epsilon = -A(r)\dot{t}^2 + B(r)\dot{r}^2 + r^2\dot{\phi}^2, \tag{2.1.8}$$

which can be rewritten as

$$\dot{r}^2 = \frac{E^2}{A(r)B(r)} - \frac{L^2}{r^2B(r)} - \frac{\epsilon}{B(r)}. \tag{2.1.9}$$

For the rest of this section we will focus on null geodesics, so for this section, $\epsilon = 0$. Eq. (2.1.9) gives an expression for r, however the r in this equation is squared. Taking the square root of this equation will result in a loss of information (in particular, the sign of the velocity at the turning point in r). Therefore, we find a different expression for r that preserves this information. To do this we make use of the Lagrangian, which is defined as

$$L = \frac{1}{2}g_{\alpha\beta}\dot{x}^\alpha\dot{x}^\beta. \tag{2.1.10}$$

For the metric given by Eq.(2.1.1), this Lagrangian becomes

$$L = \frac{1}{2}(-A(r)\dot{t}^2 + B(r)\dot{r}^2 + r^2\dot{\phi}^2). \tag{2.1.11}$$

We use the Euler-Lagrange equation in the r-direction

$$\frac{d}{d\lambda}(\frac{\partial L}{\partial \dot{r}}) = \frac{\partial L}{\partial r}. \tag{2.1.12}$$

The result of this equation is

$$p_r = \dot{r}B(r), \tag{2.1.13}$$

with

$$\dot{p}_r = \frac{1}{2}(-\frac{\partial A(r)}{\partial r}\dot{t}^2 + \frac{\partial B(r)}{\partial r}\dot{r}^2 + 2r\dot{\phi}^2). \tag{2.1.14}$$

We used the definition of the momentum in the r-direction given by

$$p_r = \frac{\partial L}{\partial \dot{r}}. \tag{2.1.15}$$

As a result, we are left with an expression for r and with an expression for p_r, which we can simplify by substituting Eq. (2.1.5), Eq. (2.1.6) and Eq. (2.1.13) into Eq. (2.1.14). The resulting system of equations of motion for null geodesics in a spherically symmetric vacuum spacetime is

$$\dot{t} = EA(r)^{-1}, \tag{2.1.16a}$$

$$\dot{\phi} = \frac{L}{r^2}, \tag{2.1.16b}$$

$$\dot{r} = p_r B(r)^{-1}, \tag{2.1.16c}$$

$$\dot{p}_r = \frac{1}{2}\Big(- \frac{E^2}{A(r)^2}\frac{\partial A(r)}{\partial r} + \frac{p_r^2}{B(r)^2}\frac{\partial B(r)}{\partial r} + \frac{2L^2}{r^3}\Big). \tag{2.1.16d}$$

This system of equations is equivalent to the geodesic equation. A derivation can be found in the Appendix.

2.2 Effective potential function and circular orbits

We will now take a look at some properties of geodesics in a spherically symmetric spacetime. We are starting with the circular orbits of the system. The radius of circular orbits is the distance between the centre of the system and a point in space for which either massless or massive particle are able to travel in a circular motion. The geodesic for these distances is a closed circle. For a black hole or black hole mimicker in equilibrium it may be possible to observe particles at these distances. The physical implementations of circular orbits will be investigated for the different types of black holes and mimickers separately in later chapters.

The circular orbits in a spherically symmetric spacetime can be determined by taking a look at the minima and maxima of the effective potential function of the system. The effective potential is defined as

$$V_{\text{eff}}(r) = -\frac{1}{2}\dot{r}^2, \tag{2.2.1}$$

which we can specify for our system by using Eq. (2.1.9). Combining these two equations results in

$$V_{\text{eff}}(r) = -\frac{E^2}{2A(r)B(r)} + \frac{L^2}{2r^2B(r)} + \frac{\epsilon}{2B(r)}. \tag{2.2.2}$$

The extreme values of the potential function Eq. (2.2.2) can be expressed by

$$-\frac{E^2}{2A(r)^2B(r)^2}(B(r)A'(r) + A(r)B'(r)) + \frac{L^2}{2r^3B(r)^2}(rB'(r) + 2B(r)) + \frac{\epsilon}{2B(r)^2}B'(r) = 0. \tag{2.2.3}$$

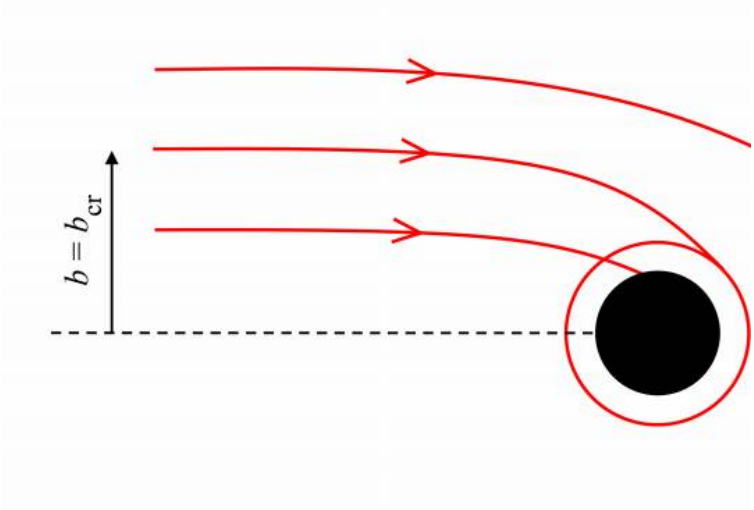

Figure 1: Photons entering a black hole system for different impact parameters. The photon with the critical impact parameter ends in circular motion around the black hole. The black disc marks the event horizon of the black hole. Figure adapted from [3].

Minima in the effective potential function correspond to stable circular orbits. Maxima on the other and correspond to unstable circular orbits. From Eq. (2.2.3) it will not be possible to determine whether we are dealing with a minimum or a maximum. This can be achieved by plotting the effective potential function of Eq. (2.2.2) or by calculating the second derivative of the potential function.

2.3 Critical impact parameter

For the remaining two properties we will only be looking at null geodesics. The impact parameter is the perpendicular distance from a photon that enters the system to the centre of the system. The impact parameter b is defined as

$$b = L/E. \tag{2.3.1}$$

Here L and E are the angular momentum and the energy of the system given by Eq. (2.1.5) and Eq. (2.1.6), respectively. The critical impact parameter of the system is the impact parameter for which the photon will precisely fall into the circular orbit around the centered object, as you can see in figure 1. For an impact parameter that is smaller than the critical impact parameter the photon will always end up inside the black hole. For an impact parameter that is bigger than the critical impact parameter the photon will end up at infinite distance from the black hole. To calculate the critical impact parameter, we use Eq. (2.1.9) for photons and rewrite it as

$$\dot{r}^2 = \frac{E^2}{r^3}\left(\frac{r^3}{A(r)B(r)} - \frac{rb^2}{B(r)}\right) \tag{2.3.2}$$

for general spherically symmetric masses. This means the critical impact parameter can be found by solving

$$\frac{d}{dr}\Big(\frac{r_{\text{circ}}^3}{A(r_{\text{circ}})B(r_{\text{circ}})} - \frac{r_{\text{circ}}b_{\text{crit}}^2}{B(r_{\text{circ}})}\Big) = 0. \tag{2.3.3}$$

This is because the critical impact parameter corresponds to the turning point of Eq (2.3.2). The turning point can be found by setting the derivative of the part between the brackets equal to zero. This is the case for Eq. (2.3.3). More information can be found in [4]. We extended the expressions in this paper for a general spacetime. In Eq. (2.3.3), b_{crit} is the critical impact parameter and r_{circ} is the radius for which the null geodesic is circular. This quantity is specified in section 2.2.

2.4 Deflection angle

The last property of the metric we will be looking at is the deflection angle. The deflection angle is the total angle of curvature of a photon path caused by the gravitational effect of the centered mass. This can be seen in figure 2. In this figure, $\delta\phi$ is the deflection angle for a photon with impact parameter b. The original path is the path for a photon with the same impact parameter in flat Minkowski space. The deflection angle in flat space is zero. We will be calculating the deflection angle in two different ways: at first directly by rewriting the equations of motion into a differential equation that can be solved by taking the power expansion of the angle. The second way is by using the Gauss-Bonnet theorem which approaches the problem mathematically using the theory of differential geometry.

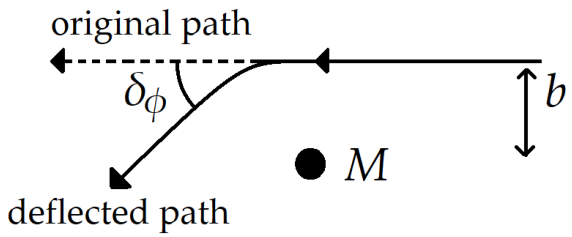

Figure 2: A photon with impact parameter b around a mass M. The original path of the photon is the path in flat Minkowski space. The deflected path is the path affected by the mass M and follows the curved spacetime. The deflection angle is given by $\delta\phi$.

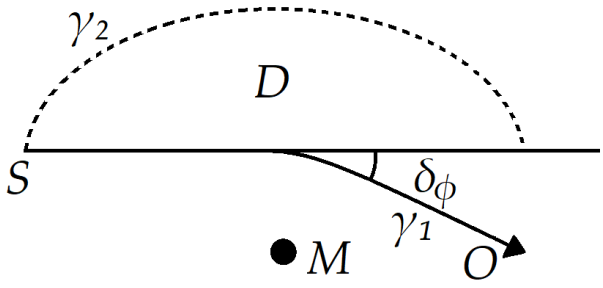

Figure 3: The deflection angle caused by gravitational lensing. The mass M causes the gravitational lensing effect. The source S sends out the photons γ_1 and γ_2. γ_1 is a photon deflected by the mass M. γ_2 is a photon in flat spacetime at infinite distance. This photon demarcates domain D. The deflection angle is given by $\delta\phi$.

2.4.1 Deflection of light by power expansion

For the first way of calculating the deflection angle we make use of the method in [5]. In this paper, the metric is defined as

$$ds^2 = -A(r)dt^2 + B(r)dr^2 + r^2C(r)d\Omega^2. \tag{2.4.1}$$

This is almost similar to the metric we use, however we set $C(r) = 1$. We are then left with

$$\frac{d^2u}{d\phi^2} + \frac{u}{B(r)} = -\frac{1}{2}u^2\frac{d}{du}\frac{1}{B(r)} + \frac{1}{2b^2}\frac{d}{du}\frac{1}{A(r)B(r)}. \tag{2.4.2}$$

In this equation $u = 1/r$. We solve this equation by taking the power expansion of u in terms of Mu_0.

$$u = u_0(\cos\phi + Mu_ou_1 + (Mu_0)^2u_2). \tag{2.4.3}$$

In this power expansion, the first terms correspond to the path a photon would take in flat spacetime, i.e., the trivial undisturbed photon path. In this equation, u_0 can be written as $u_0 = 1/b$. The higher order terms take the effect of the central massive object perturbatively into account. It is easier to leave this derivation here for now and solve Eq. (2.4.2) only for specified values of $A(r)$ and $B(r)$.

2.4.2 Gauss-Bonnet

The second way of calculating the deflection angle is by using the Gauss-Bonnet theorem. To do this we used [6], in which you can find the application of the Gauss-Bonnet theorem to gravitational lensing. The Gauss-Bonnet theorem relates the differential geometry of a surface to the topology of the surface, and in this specific case the geodesics to the curvature of space. Figure 3 shows the idea of the Gauss-Bonnet theorem. In

this figure γ_2 is a photon infinitely far away from the central massive object, following flat Minkowski space. D is the two-dimensional surface domain demarcated by γ_2. γ_1 is a photon that becomes deflected by the mass M. The deflection angle is given by $\delta\phi$. The applications of the Gauss-Bonnet theorem to gravitational lensing focuses on the equation

$$\delta\phi = -\int\int_{D_2} K dS. \tag{2.4.4}$$

The K in this equation is the trace of the extrinsic curvature of D, given by

$$\begin{aligned} K = -\exp(2(A^*(r) - B^*(r)))(&\frac{dA^*(r)}{dr}\frac{dB^*(r)}{dr} \\ &- \frac{1}{r}(\frac{dA^*(r)}{dr} - \frac{1}{r}\frac{dB^*(r)}{dr} - \frac{d^2A^*(r)}{dr^2}) \end{aligned} \tag{2.4.5}$$

and dS is given by

$$dS = \exp\left(B^*(r) - 2A^*(r)\right) r dr d\phi. \tag{2.4.6}$$

However, these equations are computed for a differently defined metric. The terms that contain a star are the ones defined in terms of the metric in the paper, the terms without star are terms we use in this thesis. The relation between these two definitions is

$$e^{2A^*(r)} = A(r) \tag{2.4.7a}$$

and

$$e^{2B^*(r)} = B(r). \tag{2.4.7b}$$

When we rewrite Eq. (2.4.5) and Eq. (2.4.6) such that it only contains non-star components, we find

$$\begin{aligned} K = -\frac{A(r)}{B(r)}\Big(&\frac{1}{4A(r)B(r)}\frac{dA(r)}{dr}\frac{dB(r)}{dr} - \frac{1}{2rA(r)}\frac{dA(r)}{dr} \\ &-\frac{1}{2rB(r)}\frac{dB(r)}{dr} + \frac{1}{2A^2(r)}(\frac{dA(r)}{dr})^2 - \frac{1}{2A(r)}\frac{d^2A(r)}{dr^2}\Big) \end{aligned} \tag{2.4.8}$$

and

$$dS = \frac{B(r)^{1/2}}{A(r)} r dr d\phi. \tag{2.4.9}$$

It is, again, easier to calculate these expressions for a specifically defined value of $A(r)$ and $B(r)$. We can still specify the boundaries of the integration in Eq. (2.4.4) in general. Because we write u in terms of cosine and the photon path has to be symmetric, we can take as integration boundaries

$$\delta\phi = -\int_{-1/2\pi}^{1/2\pi}\int_{u^{-1}}^{\infty} K dS, \tag{2.4.10}$$

in which u^{-1} is the smallest distance to the central mass and can be found during the other way of calculating the deflection angle.

3 Schwarzschild solution

The Schwarzschild metric is the simplest black hole solution to the Einstein equation. This makes it easy to directly compute the properties of the metric. Consequently, there is a vast collection of literature on the Schwarzschild spacetime and all the properties of interest in this chapter are already known. Therefore, it can be used as a nice check to the equations we have derived in chapter 2. That is why we will go through all of the properties of chapter 2 and why we will show the implementations of these properties to the Schwarzschild spacetime. Later on we will apply the results of chapter 2 to more complex black hole solutions. The Schwarzschild metric is given by

$$A(r) = B(r)^{-1} = 1 - \frac{2GM}{r}. \tag{3.0.1}$$

However, for the remainder of the thesis we will write $G = 1$. This means that we can write the Schwarzschild metric as

$$ds^2 = -(1 - \frac{2M}{r})dt^2 + (1 - \frac{2M}{r})^{-1}dr^2 + r^2 d\theta^2 + r^2 \sin^2\theta d\phi^2. \tag{3.0.2}$$

3.1 Equations of motion

We can now easily compute the equations of motion for a massless particle in a Schwarzschild metric by substituting the metric Eq. (3.0.1) into the general set of equations of motion given by Eq. (2.1.16). This gives us

$$\dot{t} = E(1 - \frac{2M}{r})^{-1}, \tag{3.1.1a}$$

$$\dot{\phi} = \frac{L}{r^2}, \tag{3.1.1b}$$

$$\dot{r} = p_r(1 - \frac{2M}{r}), \tag{3.1.1c}$$

$$\dot{p}_r = -\frac{M}{r^2}E^2(1 - \frac{2M}{r})^{-2} - p_r^2\frac{M}{r^2} + \frac{L^2}{r^3}. \tag{3.1.1d}$$

Now we will first look at some other properties in order to combine these into one plot of photon paths around a Schwarzschild metric.

3.2 Event horizon

The event horizon of a black hole is the point of no return. This means that no particle, neither massive nor massless, can leave the black hole after passing this point. The Schwarzschild coordinates we are using have two singularities: $r = 0$ and $r = 2M$. The point $r = 0$ is the black hole singularity. The point $r = 2M$ is a removable singularity. Choosing other coordinates can make this singularity disappear. However in the definition of the coordinates we chose, the singularity corresponds to the event horizon. That is why we have

$$r_{\text{horizon}} = 2M. \tag{3.2.1}$$

3.3 Circular orbits in the Schwarzschild case

We will now take a look at the circular orbits around the Schwarzschild black hole. To calculate the circular orbits and their derivatives, we solve Eq. (2.2.2) and Eq. (2.2.3) for the metric in Eq. (3.0.2). The results are

$$V_{\text{eff}}(r) = \frac{L^2}{2r^2}(1 - \frac{2M}{r}) + \frac{1}{2}\epsilon(1 - \frac{2M}{r}) - \frac{E^2}{2}, \tag{3.3.1}$$

with

$$\frac{dV_{\text{eff}}}{dr} = \frac{L^2}{r^2}(\frac{M}{r^2} - \frac{1 - \frac{2M}{r}}{r}) + \frac{M\epsilon}{r^2}. \tag{3.3.2}$$

Now we will first investigate the circular orbits of photons and then we will take a look at the circular orbits of massive particles and the physical meaning of both cases.

3.3.1 Photon ring

For the circular orbits of photons we set ϵ equal to zero. We get

$$V_{\text{eff}}(r) = \frac{L^2}{2r^2}(1 - \frac{2M}{r}) - \frac{E^2}{2}. \tag{3.3.3}$$

Figure 4 gives the plot of the effective potential stated in Eq. (3.3.3) as function of the distance r. The different graphs show the potential for varying values of the angular momentum L. Because the energy term $-E^2/2$ is independent of the radius r, it will not effect the position of the circular orbits. It is only a vertical translation of the potential graphs. Therefore, for plotting purposes, we will set this term equal to zero. There is a peak visible in figure 4. In the figure we see that this extreme value is at the same point of r for every value of L. Because this peak is a maximum, this circular orbit is unstable. To calculate the exact point of this circular orbit, we set the derivative in Eq. (3.3.2) for photons equal to zero and we find

$$r_{\text{circ,massless}} = 3M, \tag{3.3.4}$$

so there is an unstable circular orbit for photons at the point $r = 3M$. This circular orbit is called the photon ring or photon sphere. The photon sphere is unstable and it is not a physical sphere that can be detected as a result. However, physically it does play an important role. The photon sphere is the union of all closed null geodesics. In other words, there are no other closed null geodesics in a Schwarzschild spacetime such as closed ellipses. Photons tangential to the photon sphere will remain on the photon sphere. However, given that the photon sphere is unstable, small perturbations will cause the photon to either fall into or leave the black hole.

3.3.2 Innermost stable circular orbit

Let us look at massive particles now and set ϵ equal to 1 in Eq. (3.3.1). The effective potential in this case is given by

$$V_{\text{eff}}(r) = \frac{L^2}{2r^2}(1 - \frac{2M}{r}) + \frac{1}{2}(1 - \frac{2M}{r}) - \frac{E^2}{2}. \tag{3.3.5}$$

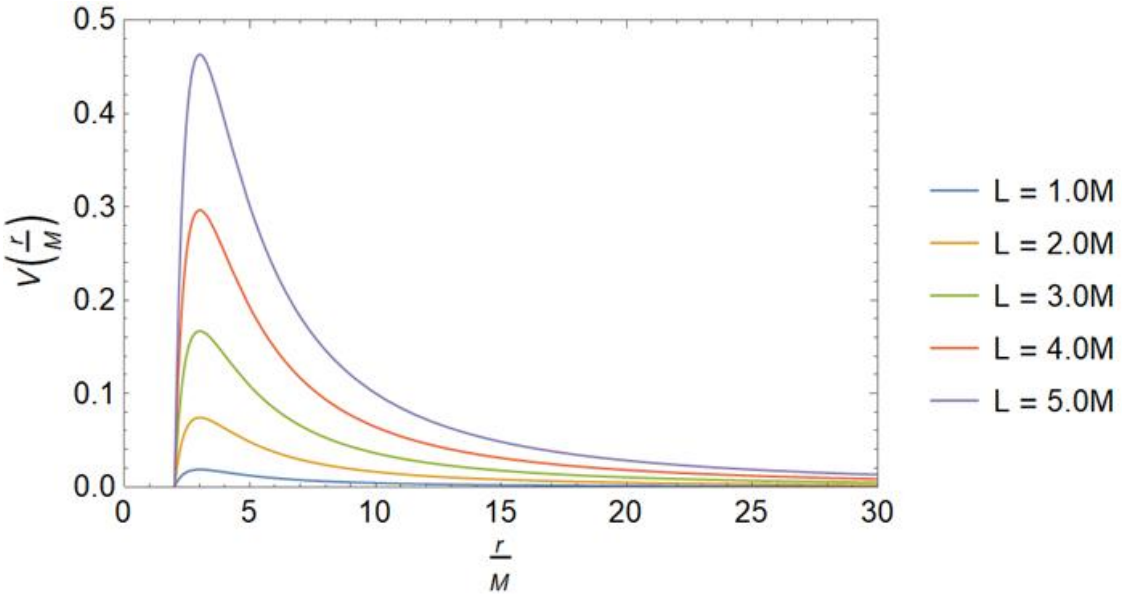

Figure 4: The effective potential function as a function of r for different values of the angular momentum. The energy term of the effective potential is set to zero.

Again, for plotting purposes, we set the $-E^2/2$ term equal to zero, because it is independent of the radius r. The plots of Eq. (3.3.5) for different values of the angular momentum L is shown in figure 5. Here we see that there is not a single peak for every value of L. We can distinguish two types of effective potential graphs. The first type is the graph for high L, which has a peak for a low value of r (an unstable orbit). There exists an additional stable orbit for a specific higher value of r. The other type of graphs have low values of L. These graphs do not have any extreme values and as a result no circular orbits. We can also approach these different cases mathematically by setting the derivative in Eq. (3.3.2) equal to zero for massive particles. The result is

$$r_{\text{circ,massive}} = \frac{L^2}{2M} \pm \frac{1}{2M}\sqrt{L^4 - 12M^2L^2}. \tag{3.3.6}$$

Indeed, we see that this equation does not have any real solutions for small values of L (i.e., small compared to M). There are two solutions to this equation for high values of L. In figure 5 we see that the graphs for high values of L indeed have two extreme values, for which the one with the smallest radius is unstable and the one with the biggest radius is stable. Therefore the plus solution of Eq. (3.3.6) corresponds to the stable orbit and the minus solution corresponds to the unstable orbit. The stable solution of Eq. (3.3.6), which has the smallest radius to the black hole, is the case for which the square root vanishes. This is the case for

$$r_{\text{ISCO}} = 6M, \tag{3.3.7}$$

which corresponds to the green line in figure 5. This orbit is called the innermost stable circular orbit (ISCO). Physically the ISCO has to be the smallest radius to the black

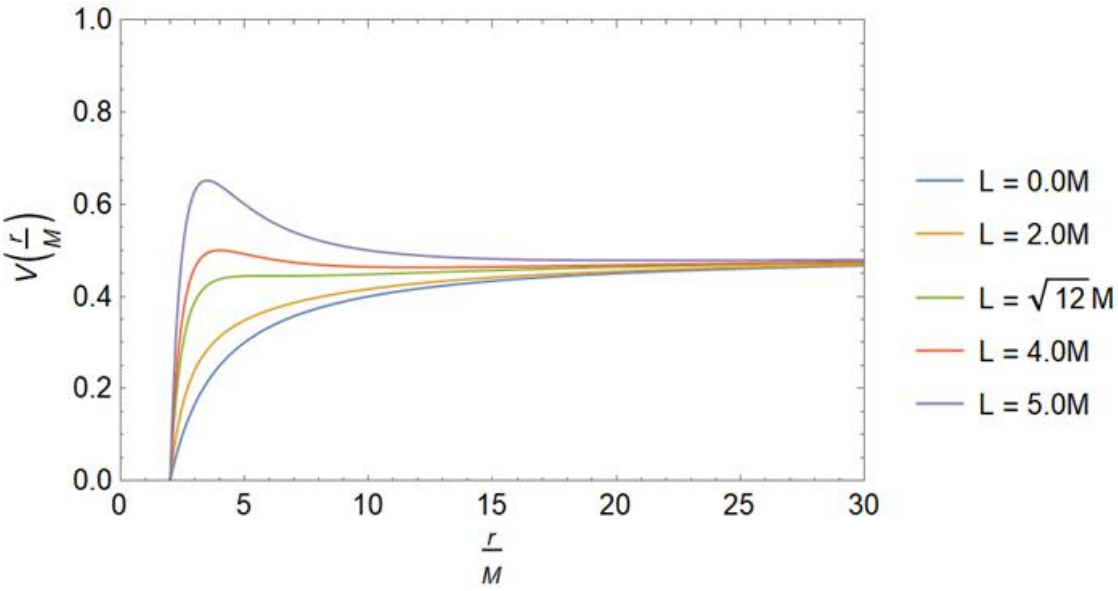

Figure 5: The effective potential plots for massive particles for different values of the angular momentum L. The peaks in the figure correspond to unstable circular orbits. The green line is the turning point between graphs that do and the graphs that do not have any circular orbits. The point where the green graph has derivative zero is called the innermost stable circular orbit.

hole for which matter can be found in a stable orbit around the black hole. This means that the accretion disc around a Schwarzschild black hole can not be attached to the black hole, the accretion disc has to start at the ISCO.

3.4 Photon paths around a Schwarzschild black hole

For the rest of this chapter we are going to focus on null geodesics. Figure 6 gives the photon paths around the Schwarzschild black hole for different impact parameters. The black disc in figure 6 indicates the area inside of the event horizon calculated in section 3.2. The gray area indicates the inside of the photon sphere, calculated in section 3.3.1. The photon paths are calculated by numerically solving the equations of motion in Eq. (3.1.1). This was done in Mathematica 12 using the built-in RK4 numerical integrator. To create this plot, we shoot photons on the black hole from the downside of the figure. Every line represents a photon path and the distance between the separate photons is $1M$.

3.5 Critical impact parameter

We will now take a look at some other properties of the Schwarzschild black hole. At first we calculated the critical impact parameter. To calculate the critical impact parameter we solved Eq. (2.3.3) for the metric given by Eq. (3.0.2). This resulted in

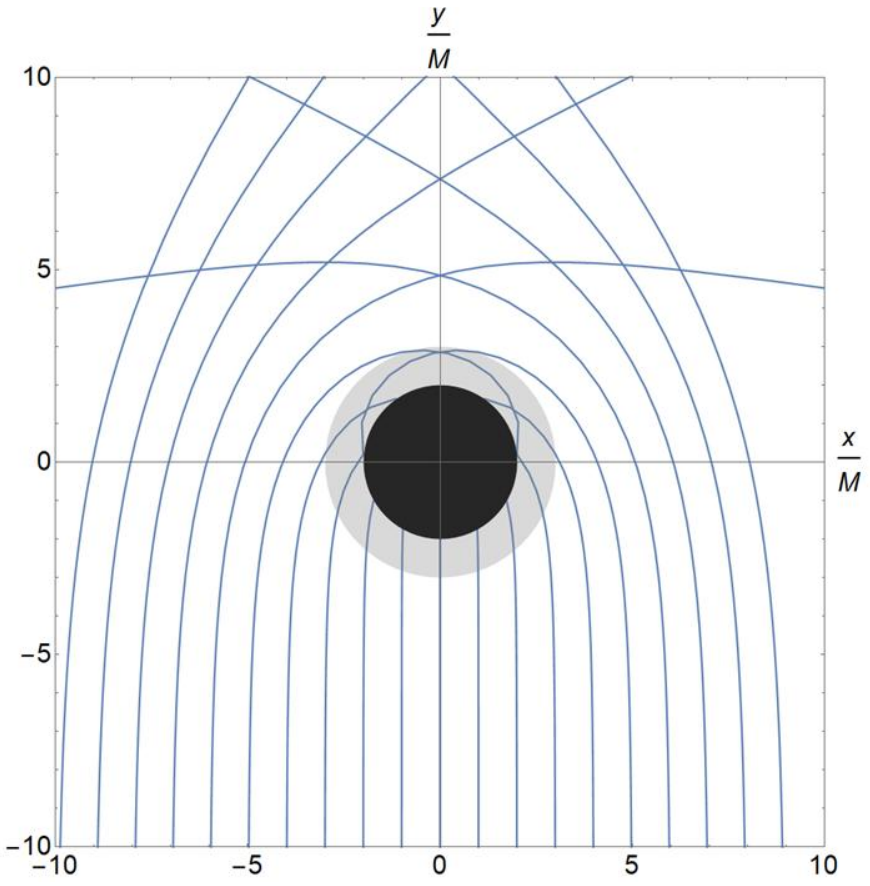

Figure 6: Photon paths around a Schwarzschild black hole for different impact parameters. The photons were shot on the black hole from below. The black disc indicates the area inside of the event horizon and the gray disc the area inside of the photon ring. The coordinates x and y are the Cartesian coordinates calculated by $x = r\cos\phi$ and $y = r\sin\phi$.

the equation

$$3r_{\text{circ}}^2 - b_{\text{crit}}^2(1 - \frac{2M}{r_{\text{circ}}} + r_{\text{circ}}\frac{2M}{r_{\text{circ}}^2}) = 0. \tag{3.5.1}$$

The solution of this equation is

$$b_{\text{crit}} = \sqrt{3}r_{\text{circ}} = 3\sqrt{3}M, \tag{3.5.2}$$

in which r_{circ} is the photon sphere calculated in section 3.3.1. In figure 7 we see a photon with an impact parameter of $3\sqrt{3}M$. As expected, the black hole catches the photon in a circular orbit. This plot is not constructed by using the system of equations of motion given by Eq. (3.1.1). Due to numerical errors the photon plotted by the regular equations of motion will not stay in a circular orbit. Remember that this orbit is unstable. That is why we plotted the photon path in figure 7 using the analytical solution to the equations of motion, which for this particular impact parameter takes the simple form

$$\frac{M}{r(\phi)} = \frac{1}{3} - \frac{1}{1 \pm \cosh\phi}. \tag{3.5.3}$$

For generic impact parameters, the analytic results are also known but are more complicated and involve the Weierstrass elliptic functions [7]. We have checked that all the numerical solutions obtained in this section match the analytic solutions (within the numerical error range). This served as an additional check to our numerical methods for finding the equations of motion. Given the relatively complicated form, we shall not include the analytic expressions. In figure 7 we see that the photon indeed circles the black hole at a distance of $3M$, which is distance of the photon sphere.

3.6 Deflection angle

In this section we will look at the deflection angle in the Schwarzschild case. We will calculate the deflection angle using both methods described in section 2.4.

3.6.1 Deflection of light by power expansion

Solving Eq. (2.4.2) for the Schwarzschild metric has already been described in [5]. We will give a summary of how to solve this system. Eq. (2.4.2) for the Schwarzschild case reduces to

$$\frac{d^2u}{d\phi^2} + u = 3Mu^2. \tag{3.6.1}$$

To solve this system we write u as in Eq. (2.4.3) and ignore all the higher terms of u. We now sort all terms of u with the same order of Mu_0 and find the system of equations

$$\frac{d^2u_1}{d\phi^2} + u_1 = 3\cos^2\phi, \tag{3.6.2}$$

$$\frac{d^2u_2}{d\phi^2} + u_2 = 6u_1\cos\phi. \tag{3.6.3}$$

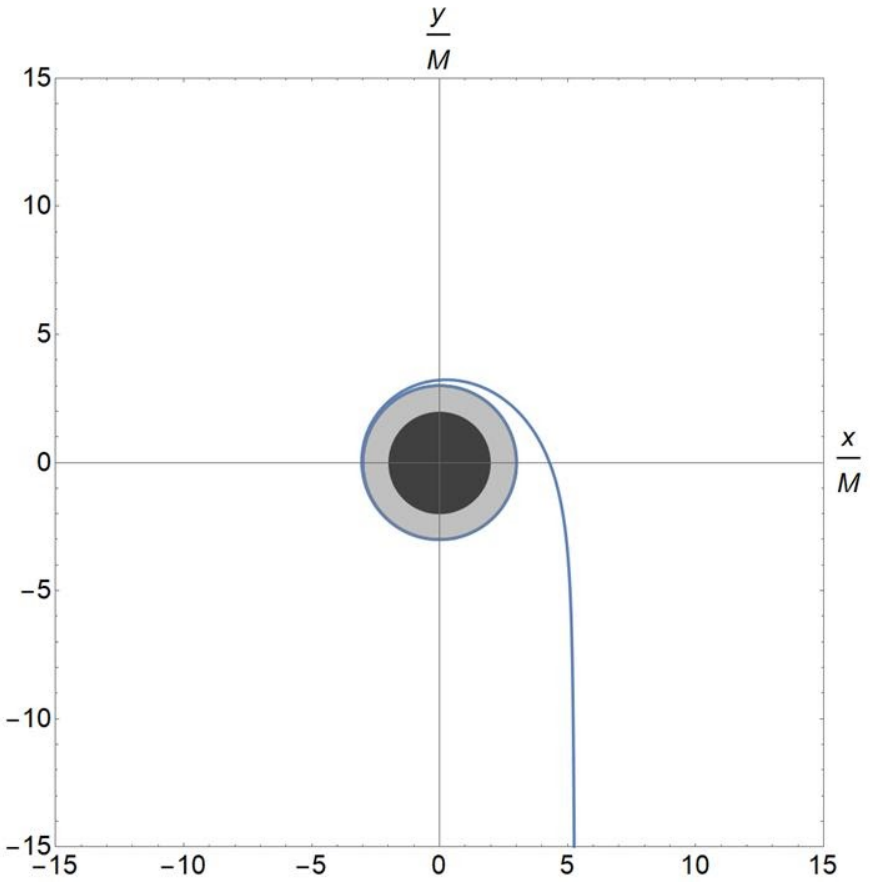

Figure 7: A photon entering a Schwarzschild black hole system with the critical impact parameter. The plot is constructed by using Eq. (3.5.3). The photon circles the outer radius of the gray area around the black hole, so it stays in the photon sphere.

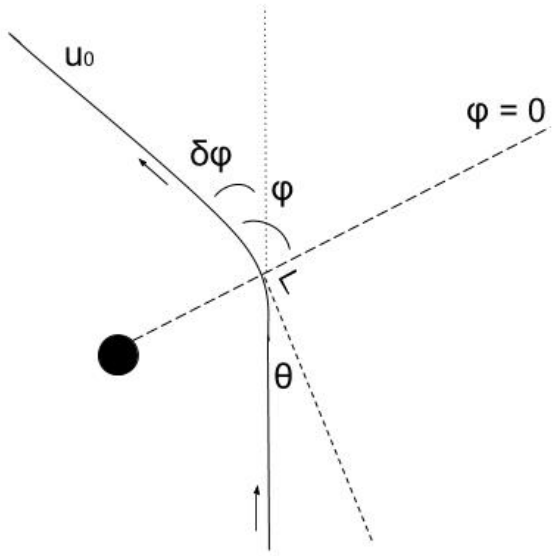

Figure 8: A deflected photon in a Schwarzschild metric. The deflection angle is given by $\delta\phi$. u tends to zero when r goes to infinity. The angle ϕ can be expressed by $\phi = \pi/2 + \theta$.

The solutions to this system are

$$u_1 = \frac{3 - \cos 2\phi}{2}, \tag{3.6.4}$$

$$u_2 = \frac{15}{4}\phi \sin\phi + \frac{3}{16}\cos 3\phi. \tag{3.6.5}$$

We can put these solutions into Eq. (2.4.3) and find

$$u = u_0\Big(\cos\phi + Mu_o\frac{3 - \cos 2\phi}{2} + (Mu_0)^2(\frac{15}{4}\phi\sin\phi + \frac{3}{16}\cos 3\phi)\Big). \tag{3.6.6}$$

We now use the fact that u goes to zero for $\phi = \pi/2 + \theta$. This is shown in figure 9. Consequently, we can take the Taylor series of this value of u around zero. This Taylor expansion turns out to be

$$\theta = 2Mu_0 + M^2u_0^2(\frac{15\pi}{8}). \tag{3.6.7}$$

Because the deflection angle is symmetric around $\phi = 0$, we have to multiply the angle θ by two. We get

$$\delta\phi = 4Mu_0 + M^2u_0^2(\frac{15\pi}{4}). \tag{3.6.8}$$

The relation between u_0 and the impact parameter is $u_0 = 1/b$. We can now write the deflection angle as a function of the impact parameter

$$\delta\phi = \frac{4M}{b} + \frac{M^2}{b^2}(\frac{15\pi}{4}). \tag{3.6.9}$$

3.6.2 Gauss-Bonnet

We now calculate the deflection angle with the Gauss-Bonnet theorem to check if both methods give the same results. Calculating the deflection angle using this method in a Schwarzschild metric has already been done in [6], however in this paper the deflection angle is only derived to leading order. In our derivation we calculate the deflection angle to second order to compare it to the deflection angle calculated in the last section. To calculate the deflection angle, we substitute the Schwarzschild metric into Eq. (2.4.8) and get

$$K = -\frac{3M^2}{r^4} + \frac{2M}{r^3}. \tag{3.6.10}$$

We substitute the Schwarzschild metric in Eq. (2.4.8) and get

$$dS = (1 - \frac{2M}{r})^{-3/2} r dr d\phi. \tag{3.6.11}$$

We then have

$$KdS = -\frac{2M}{r^2(1 - \frac{2M}{r})^{3/2}}(1 - \frac{3M}{2r}) dr d\phi. \tag{3.6.12}$$

We assume that the distance between the photon and the black hole goes to infinity. We can therefore take the numerical expansion for r goes to infinity of KdS in the first two terms. The result is

$$KdS = -\frac{2M}{r^2} - \frac{3M^2}{r^3} dr d\phi. \tag{3.6.13}$$

The integral in equation Eq. (2.4.10) becomes

$$\delta\phi = -\int_{-1/2\pi}^{1/2\pi} \int_{u^{-1}}^{\infty} -\frac{2M}{r^2} - \frac{3M^2}{r^3} dr d\phi. \tag{3.6.14}$$

As said before, the u in this equation can be used from the other way of calculating the deflection angle. Because we want to calculate only the first two terms we can use the first two terms of u, given by Eq. (3.6.6), which is

$$u = \frac{\cos\phi}{b} + \frac{M}{b^2}\frac{3 - \cos 2\phi}{2}. \tag{3.6.15}$$

The solution of the integral given in equation 3.6.14 for u given by Eq. (3.6.15) is

$$\delta\phi = \frac{4M}{b} + \frac{M^2}{b^2}(\frac{15\pi}{4}), \tag{3.6.16}$$

which agrees with the deflection angle obtained in section 3.6.1. The deflection angle is plotted in figure 9 and 10 under different circumstances. In figure 9 the deflection angle and photon path for a photon with impact parameter $20M$ is plotted. In this figure you see the deflection angle for the leading order term only and for the leading and next-to-leading order term. The leading plus next-to-leading order term is a better approximation for the deflection angle than only the leading order term. In figure 10 the deflection angle and photon path is plotted for photons with different impact parameters. Because we made the assumption that the distance between the photon and the black hole goes to infinity, the approximation of the deflection angle gets worse for smaller impact parameters. That is because the higher terms in the deflection angle increase for smaller impact parameters.

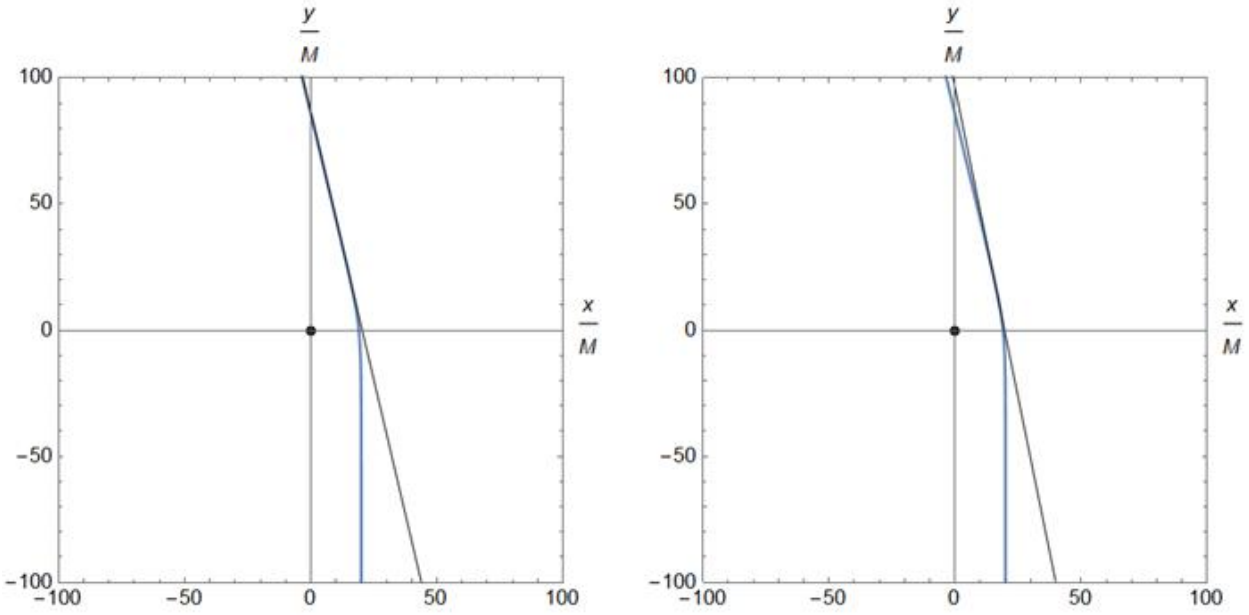

Figure 9: The deflection angle (black line) and photon path (blue line) for a photon with an impact parameter of $b = 20$. The deflection angle in the left plot consists of both the linear and quadratic term. The deflection angle of the photon in the right plot consists of only the linear term. There is a small deviation between the deflection angle and the photon path in the right plot. This is not the case for the left plot. This means that the linear plus quadratic term of the deflection angle is indeed a better approximation of the photon path than only the linear term.

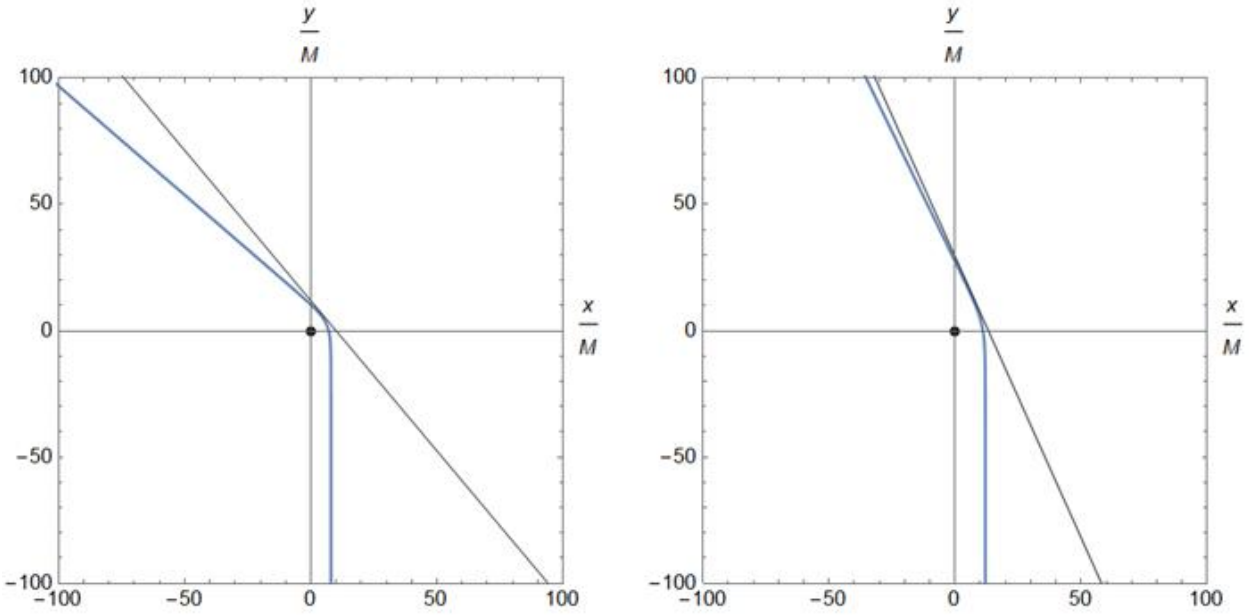

Figure 10: The deflection angle (black line) and photon path (blue line) of two photons with different impact parameter. The photon of the plot on the left side has an impact parameter of $b = 8$. The photon of the plot on the right side has an impact parameter of $b = 12$. There is a bigger deviation between the photon paths and the deflection angle of photons with a smaller impact parameter, because the influence of the higher terms in the deflection angle increases.

4 Reissner-Nordström solution

We will now take a look at Reissner-Nordström black holes. The Reissner-Nordström metric is an extension of the Schwarzschild metric. This generalization of the Schwarzschild spacetime not only depends on the mass, but also depends on the electric charge. Thus, the Reissner-Nordström black hole is a charged black hole for which we have

$$A(r) = B(r)^{-1} = 1 - \frac{2M}{r} + \frac{Q^2}{r^2}. \tag{4.0.1}$$

Which means that the metric is given by

$$ds^2 = -(1 - \frac{2M}{r} + \frac{Q^2}{r^2})dt^2 + (1 - \frac{2M}{r} + \frac{Q^2}{r^2})^{-1}dr^2 + r^2 d\theta + r^2 \sin^2\theta d\phi^2. \tag{4.0.2}$$

In this metric, Q is the charge of the black hole. We assume that there is no magnetic charge. This metric can easily be extended by replacing Q^2 with $P^2 + Q^2$, where P is the magnetic charge. We see that the difference of the metric is proportional to $1/r^2$, thus the correction term decays quickly for large distances. Therefore, for $r >> 0$, many of the properties of Reissner-Nordström (RN) black hole are well approximated by the Schwarzschild solution.

4.1 Equations of motion

Just as in chapter 3, we substitute the metric into the general system of equations of motion, given by Eq. (2.1.16). This gives

$$\dot{t} = E(1 - \frac{2M}{r} + \frac{Q^2}{r^2})^{-1}, \tag{4.1.1a}$$

$$\dot{\phi} = \frac{L}{r^2}, \tag{4.1.1b}$$

$$\dot{r} = p_r(1 - \frac{2M}{r} + \frac{Q^2}{r^2}), \tag{4.1.1c}$$

$$\dot{p_r} = \frac{E^2}{r^2}(1 - \frac{2M}{r} + \frac{Q^2}{r^2})^{-2}(Mr - Q^2) - \frac{p_r^2}{r^3}(Mr - Q^2) + \frac{L^2}{r^3}. \tag{4.1.1d}$$

4.2 Horizons

The location of the event horizon can be derived by setting the time component of the metric equal to zero, in other words, $A(r)$ needs to vanish at the horizon. This is the case for

$$1 - \frac{2M}{r} + \frac{Q^2}{r^2} = 0, \tag{4.2.1}$$

which has the solution

$$r_{\text{horizon}} = M \pm \sqrt{M^2 - Q^2}. \tag{4.2.2}$$

We can distinguish three types of solutions to Eq. (4.2.2). In case of $M > Q$ the RN metric has two horizons. This type of RN black hole is the most likely one in case of gravitational collapse. The outer horizon of the black hole has the same behaviour as

the event horizon for the Schwarzschild solution. This means that the outer horizon behaves like the point of no return. At this radius, r switches from being a spacelike coordinate to being a timelike coordinate. As a consequence, the particle or photon can only move in the direction of decreasing r. At the inner horizon the r coordinate switches back to being spacelike, which means that the photon can move in any direction. Therefore it is not necessary for the photon to reach the singularity at $r = 0$. More information about this can be found in [8].

The case $M = Q$ is called the extremal case. In this case there will only be one horizon given by $r = M$. However, this is not an event horizon in the sense that it behaves like a point of no return. The r coordinate on both sides will be spacelike. This case is very unstable, this means that adding a little bit of mass causes the situation to fall back into the case $M > Q$.

The last case we are left with is $M < Q$. Now there will not be any horizon shielding the singularity. Consequently, we call the point $r = 0$ a naked singularity, which is not an actual black hole.

4.3 Circular orbits in the RN case

We will now take a look at the circular orbits for both massive and massless particles. To calculate the circular orbits and their derivative, we use Eq. (2.2.2) and Eq. (2.2.3). For the RN metric this potential function turns out to be

$$V_{\text{eff}}(r) = \frac{L^2}{2r^2}(1 - \frac{2M}{r} + \frac{Q^2}{r^2}) + \frac{1}{2}\epsilon(1 - \frac{2M}{r} + \frac{Q^2}{r^2}) - \frac{E^2}{2}, \tag{4.3.1}$$

with

$$\frac{dV_{\text{eff}}}{dr} = \frac{L^2}{r^2}(\frac{3M}{r^2} - \frac{2Q^2}{r^3} - \frac{1}{r}) + \frac{1}{2}\epsilon(\frac{2M}{r^2} - \frac{2Q^2}{r^3}). \tag{4.3.2}$$

We now treat the massless and massive case separately.

4.3.1 Photon ring

For massless particles, Eq. (4.3.1) reduces to

$$V_{\text{eff}}(r) = \frac{L^2}{2r^2}(1 - \frac{2M}{r} + \frac{Q^2}{r^2}) - \frac{E^2}{2}. \tag{4.3.3}$$

This potential function is plotted in figure 11. In This figure we see that the radius of the photon ring is affected by the charge of the black hole. In chapter 3 we saw that the photon ring does not depend on the value of the angular momentum L. This is also the case for the RN metric. As a consequence, we can choose a constant value of L. In figure 11 we set $L = 3M$. In this figure we can see that for the case $M > Q$ there is an unstable photon ring for which the radius depends on the charge of the black hole. The potential graph also has a (very low) minimum for every value of Q, which corresponds to a stable circular orbit. For the extremal case where $M = Q$,

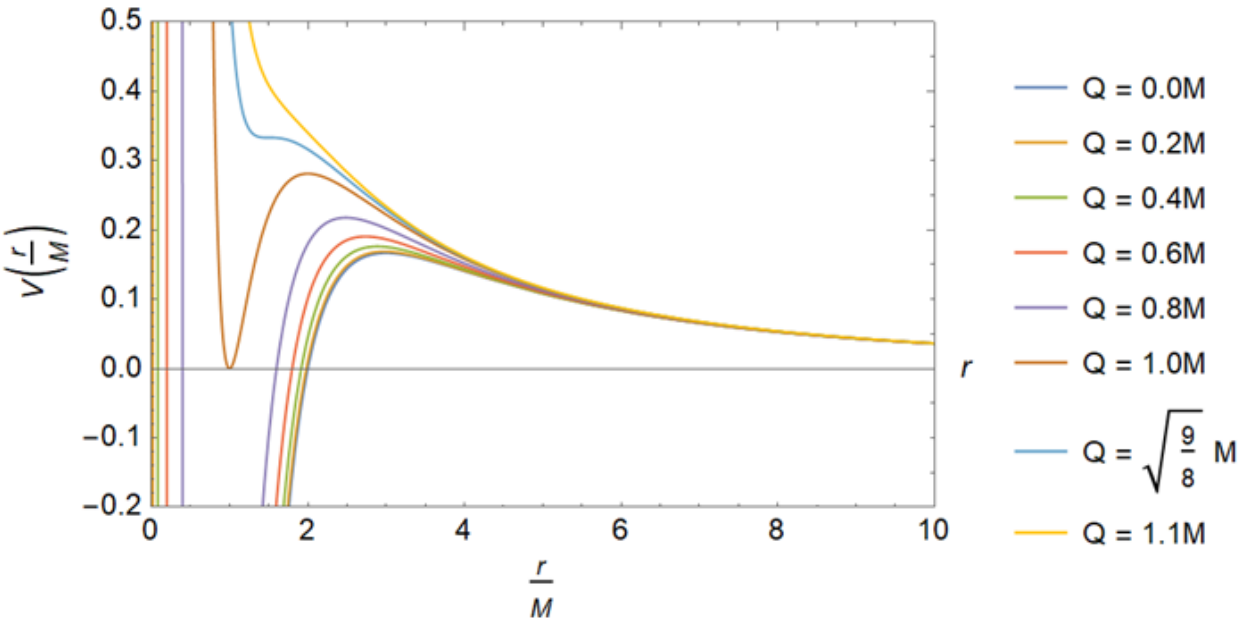

Figure 11: The potential function of photons in a Reissner-Nordström metric with different values for Q. The energy of the photons is set equal to zero and the angular momentum is set equal to 3. The photons for which the black hole has a charge smaller than the mass have a minimum and maximum, however the minima are inside of the horizon so they are not physically relevant. Black holes for which the mass is equal to or smaller than the charge, the minimum does have a physical meaning. The potential plots for even higher values of the charge does not have any extreme values.

there is both an unstable circular orbit and a stable circular orbit. For $M < Q$, the effective potential loses its extreme values, meaning that for higher values of Q, there are no photon rings. We will now view the effective potential function mathematically in order to calculate the exact point of the extreme values. Eq (4.3.2) for photons becomes

$$\frac{dV_{\text{eff}}}{dr} = \frac{L^2}{r^2}\left(\frac{3M}{r^2} - \frac{2Q^2}{r^3} - \frac{1}{r}\right). \tag{4.3.4}$$

The roots of this equation are given by

$$r_{\text{circ}} = \frac{3}{2}M \pm \frac{1}{2}\sqrt{9M^2 - 8Q^2}. \tag{4.3.5}$$

In case $M > Q$, Eq. (4.3.5) has two solutions. The minus solution of this equation corresponds to the local minimum we saw in figure 11. However, the radius of this photon ring is smaller than the outer horizon of the black hole. This means that the minus solution of the circular orbit solution Eq. (4.3.5) does not correspond to a photon ring outside of the event horizon of the black hole. The plus solution of Eq. (4.3.5)

corresponds to an unstable photon ring.

For $M = Q$, Eq. (4.3.5) also has two solutions, $r = M$ and $r = 2M$. In figure 11 we see that the solution $r = M$ corresponds to a stable photon ring and $r = 2M$ corresponds to an unstable photon ring. In section 4.2 we saw that the radius $r = M$ is also the horizon of this type of RN black hole.

Black holes that have a charge for which $Q > M$ and $Q < \sqrt{\frac{9}{8}}M$ have two solutions to Eq. (4.3.5), meaning that this type of black hole solution does have two photon rings such that the inner photon ring is stable and the outer one is unstable. However, this solution does not have an event horizon, as we saw in section 4.2. Black holes with $Q = \sqrt{\frac{9}{8}}M$ have one unstable photon ring for $r = 3/2M$. For $Q > \sqrt{\frac{9}{8}}M$, the naked singularity does not have any circular orbits.

4.3.2 Innermost stable circular orbit

For massive particles, Eq. (4.3.1) becomes

$$V_{\text{eff}}(r) = \frac{L^2}{2r^2}(1 - \frac{2M}{r} + \frac{Q^2}{r^2}) + \frac{1}{2}(1 - \frac{2M}{r} + \frac{Q^2}{r^2}) - \frac{E^2}{2}, \tag{4.3.6}$$

and its radial derivative is

$$\frac{dV_{\text{eff}}}{dr} = \frac{L^2}{r^2}(\frac{3M}{r^2} - \frac{2Q^2}{r^3} - \frac{1}{r}) + \frac{1}{2}(\frac{2M}{r^2} - \frac{2Q^2}{r^3}). \tag{4.3.7}$$

This potential function depends on both the charge Q and the angular momentum L. The radius for which the derivative of the potential vanishes can not be written as a simple expression. However, it is clear from this expression that the higher the angular momentum, the smaller the contribution of the mass. This implies that for high values of the angular momentum, the potential graphs will reach the massless solutions. To gain intuition on the behaviour of the ISCO in a RN metric, we calculated the radius of the ISCO for specific values of Q. We did his by finding a value of L such that there was only one corresponding radius r for which the effective potential function has a extreme values. The results are shown in table 1 and are plotted in figure 12. We see that the ISCO shifts to the lower values of r for higher values of Q. We found the ISCO for the extremal case with $Q = M$ to be at $r = 4M$. This means that for an RN black hole case the ISCO is between the $r = 4M$ and $r = 6M$, with $r = 4M$ corresponding to the $Q = M$ extremal case and $r = 6M$ corresponding to the $Q = 0$ Schwarzschild case. We took $0 \leq Q \leq M$ here. We conclude that, for larger values of Q, the radius of the ISCO decreases. The distance between the black hole and its accretion disc therefore gets smaller.

4.4 Photon paths around a RN black hole

For the rest of this chapter we focus on null geodesics. To make a photon path plot for the RN metric, we combine the results from section 4.1, 4.2 and 4.3. In figure 13 a

Q	L^2	ISCO radius r
0.0	12.0	6.0M
0.2	11.87	5.9M
0.4	11.46	5.8M
0.6	10.74	5.4M
0.8	9.66	4.9M
0.9	8.93	4.5M
1.0	8.0	4.0M

Table 1: The radius of the ISCO and the corresponding angular momentum L for different values of charge Q in a Reissner-Nordström metric for massive particles.

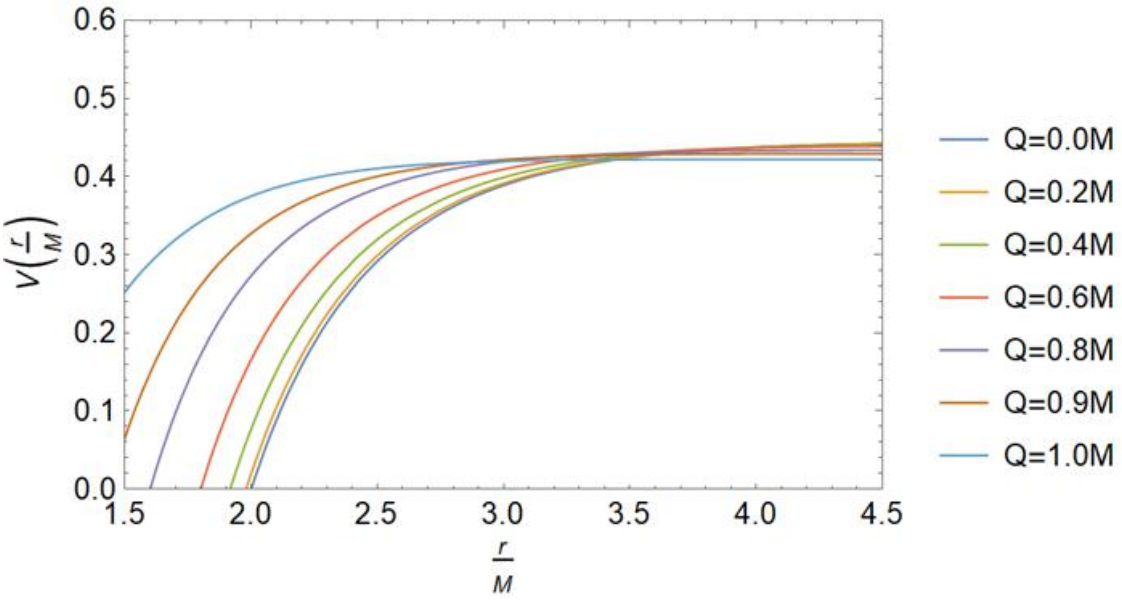

Figure 12: The potential function for different values of the charge Q in a Reissner-Nordström metric for massive particles. For higher values of Q, the potential plot shifts to the left. This causes the ISCO to shift to lower values of r for higher values of Q.

black hole is plotted with charge $Q = 0.8M$. The black disc represents the area inside the outer horizon at $r = 1.6M$, which can be calculated with Eq. (4.2.2). The gray disc represents the area inside the photon ring. The photon ring can be calculated with Eq. (4.3.5). For a charge of $Q = 0.8M$ this becomes $r = 2.5M$. We can conclude from comparing figure 13 to figure 6, which shows the photon paths in a Schwarzschild spacetime, that the radius of the horizon as well as the photon ring has decreased. We also see that the gravitational pull of the photons paths towards the black hole has decreased. The photon paths are affected less by the black hole. This means that the charge of the black hole has an opposite effect on the horizon, photon ring and photon paths as the mass of the black hole has.

In figure 14 we see the photon paths around a black hole in the extremal case, for which we have $Q = M$. For the extremal case we have seen in previous sections that the horizon is at $r = M$ and there is a photon ring is at $r = M$ and one at $r = 2M$. This is indicated in figure 14 with the black and gray disc. We see that the size of the black hole has decreased. Also the gravitational pull has decreased even more than in the $Q = 0.8M$ case. In figure 14 we see that one of the photons exactly falls into the photon ring, which is the reason for the blue circles around the photon ring.

Figure 15 gives the photon paths for the naked singularity $Q > M$ case. In this plot we have set $Q = 2.0M$. In this case there is no horizon and there is also no photon ring. We see that the singularity actually has a repellent effect on the photon paths with a low impact parameter. For high impact parameter photon paths, the $1/r$ mass term in the metric Eq. (4.0.2) is the leading term, in contrast to the $1/r^2$ electromagnetic term. This causes a gravitational pull.

4.5 Critical impact parameter

To calculate the critical impact parameter for the RN case we use Eq. (4.3.3). Which gives

$$3r_{\text{circ}}^2 - b_{\text{crit}}^2(1 - \frac{2M}{r_{\text{circ}}} + \frac{Q^2}{r_{\text{circ}}^2} + r_{\text{circ}}(\frac{2M}{r_{\text{circ}}^2} - \frac{2Q^2}{r_{\text{circ}}^3})) = 0. \tag{4.5.1}$$

The result of this equation is

$$b_{\text{crit}} = \sqrt{\frac{3r_{\text{circ}}^4}{r_{\text{circ}}^2 - Q^2}}. \tag{4.5.2}$$

In this equation, r_{circ} is given by Eq. (4.3.5). Of course it is only possible to calculate the critical impact parameter for cases that have a photon ring. We will verify the result by calculating the critical impact parameter for some values of Q and plotting the corresponding photon path. In figure 16 we see a black hole with charge $Q = 0.2M$. For this value the photon ring has a radius of $r_{\text{circ}} = 2.97M$. Eq. (4.5.2) then gives a critical impact parameter of $b_{\text{crit}} = 5.16M$. Figure 17 shows the photon path with this

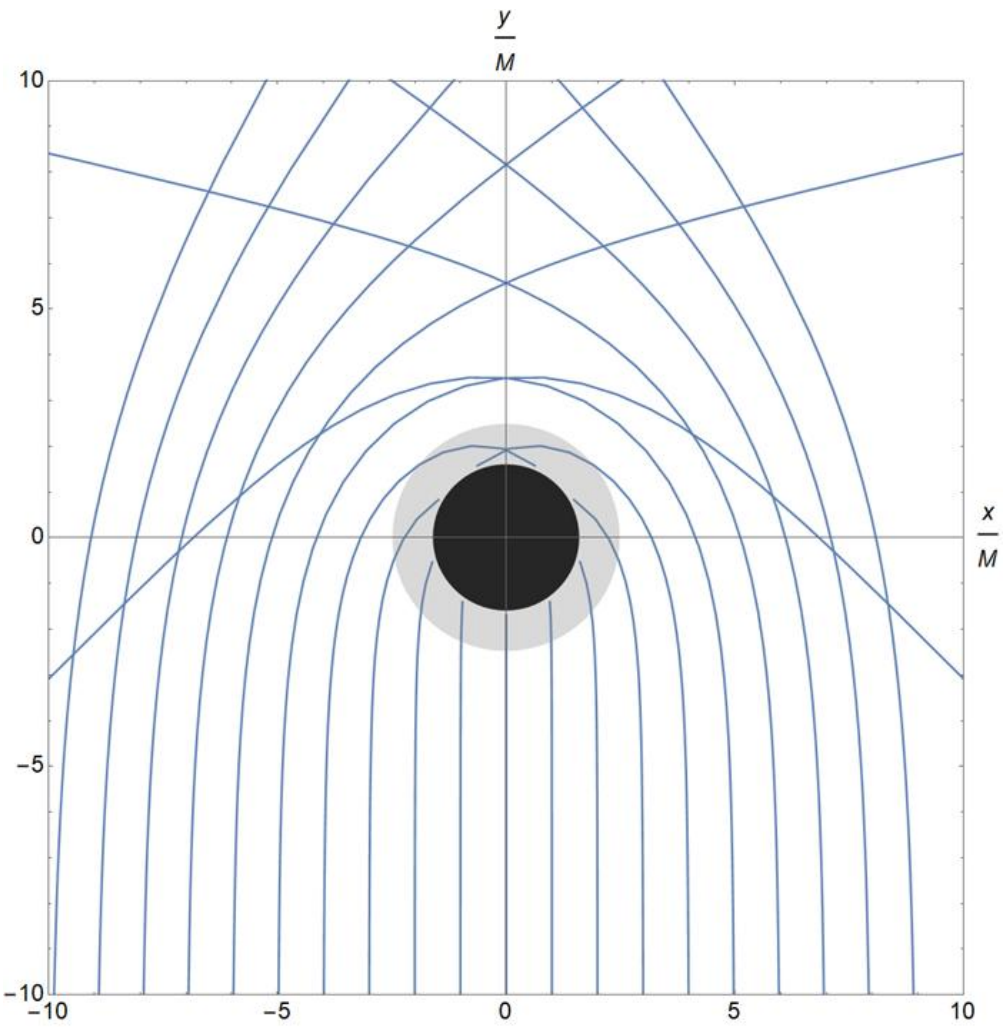

Figure 13: The photon paths around a Reissner-Nordström black hole with charge $Q = 0.8M$. The black disc indicates the inside of the outer horizon of the black hole. The gray disc indicates the inside of the photon sphere around the black hole. The radius of the horizon and photon sphere, and the gravitational pull around the black hole are all decreased compared to the Schwarzschild case.

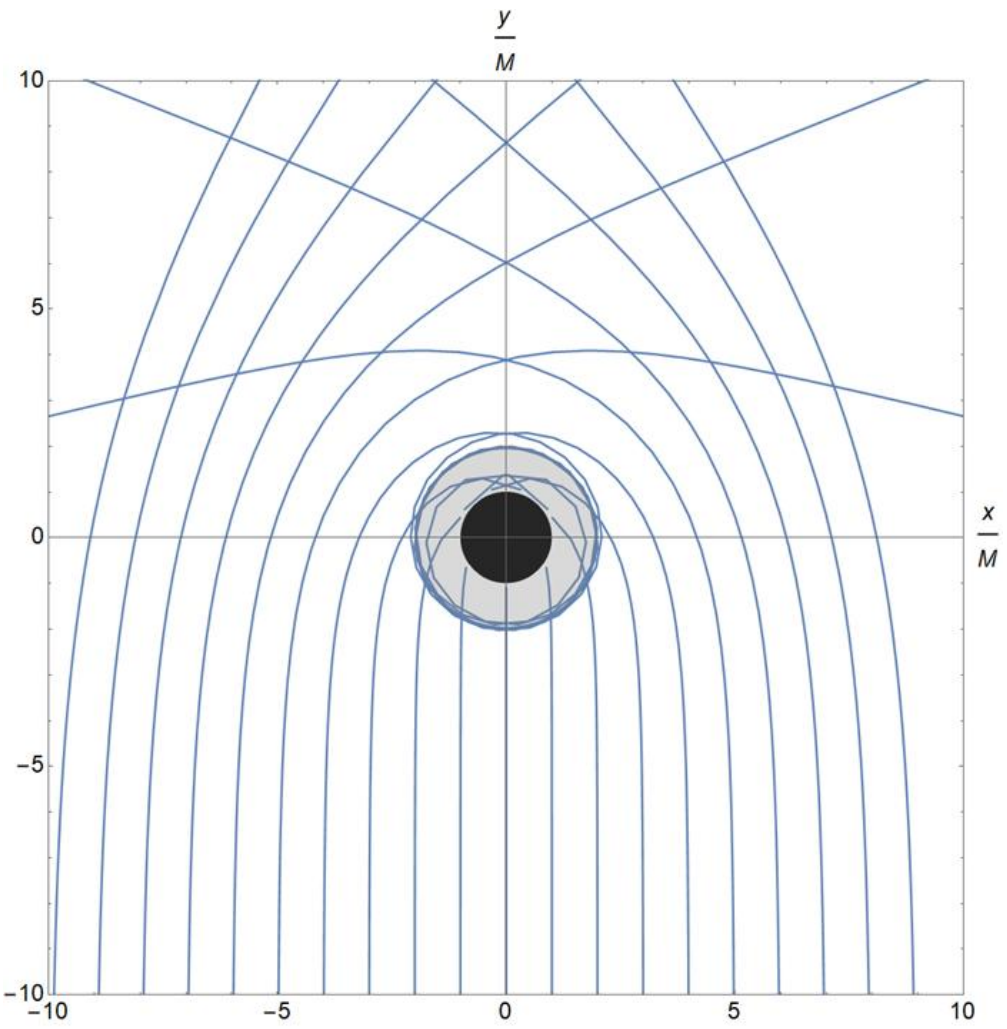

Figure 14: The photon paths around a black hole in the extremal $Q = M$ case. The black disc indicates the inside of the horizon (even though this is not an event horizon and it does not behave as a point of no return). The gray area indicates the inside of the photon ring. One of the photon paths gets stuck in the photon ring, causing the blue circles around the gray disc.

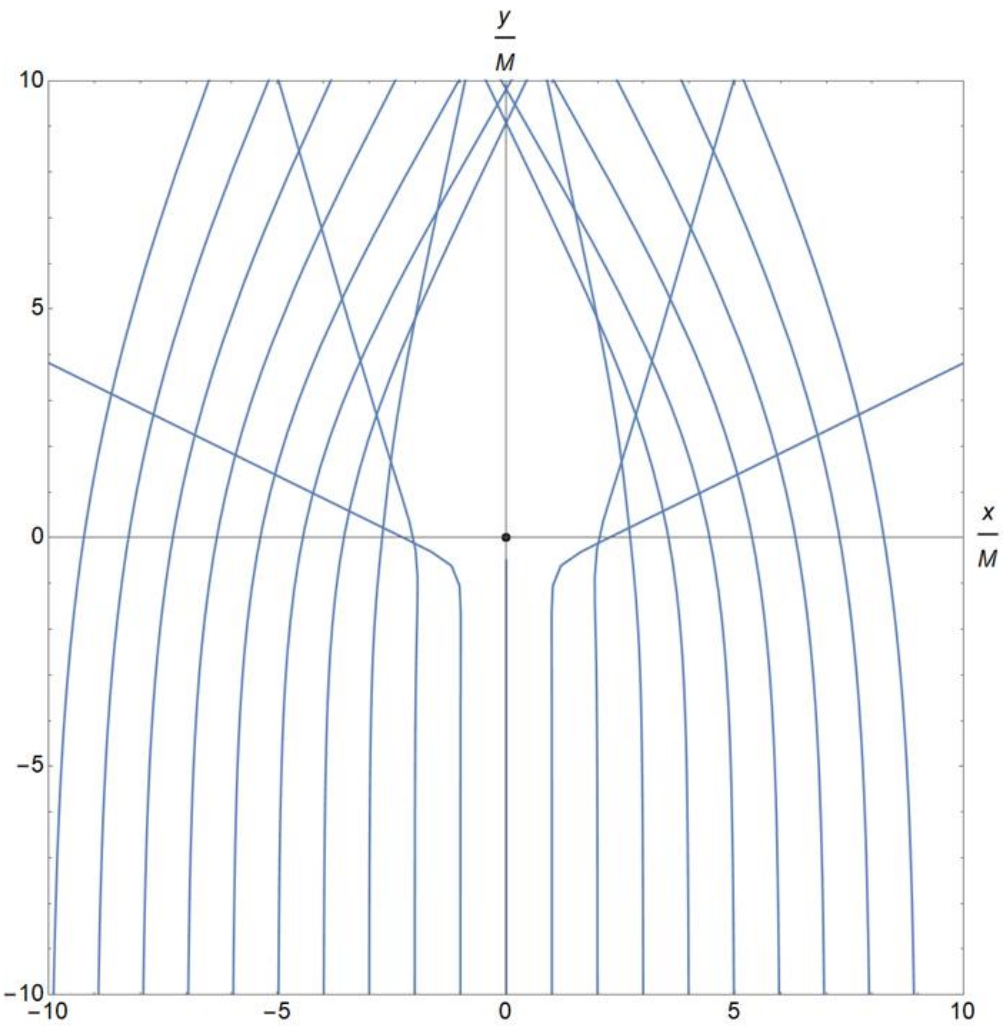

Figure 15: Photon paths around a naked singularity according to the Reissner-Nordström metric. The naked singularity has a charge $Q = 2.0M$. The naked singularity does not have a horizon or photon ring. The singularity is repelling for low impact parameter photon paths and attracting for high impact parameter photons.

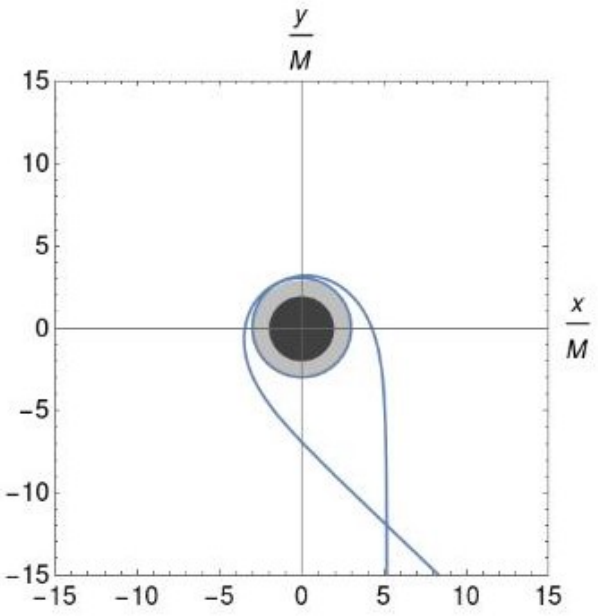

Figure 16: A photon path around a Reissner-Nordström black hole with an impact parameter that is equal to the critical impact parameter. The RN black hole has a charge of $Q = 0.2M$. The corresponding critical impact parameter is approximately $b_{\text{crit}} = 5.16M$. The photon enters the photon ring, however because of the instability of the photon ring in combination with numerical error, the photon also leaves the black hole and goes back into space.

impact parameter and we see that it indeed approximates the critical impact parameter. The photon falls out of the photon ring, because of the instability of the photon ring and the numerical errors.
In figure 17 we have plotted a black hole with charge $Q = 0.8M$. For this charge the photon ring has a radius $r = 2.48M$ and the critical impact parameter has a value of $b_{\text{crit}} = 4.55M$. In figure 17 we have plotted a photon path with this impact parameter and we yet again see that it approximates the critical impact parameter. For the extremal case $Q = M$, Eq. (4.5.2) gives a critical impact parameter of $b_{\text{crit}} = 4M$. This corresponds with figure 14, which shows that the photon with impact parameter $4M$ falls into the photon ring.

4.6 Deflection angle

We now calculate the deflection angle in an RN metric using two different methods, so we can compare the results to both strategies.

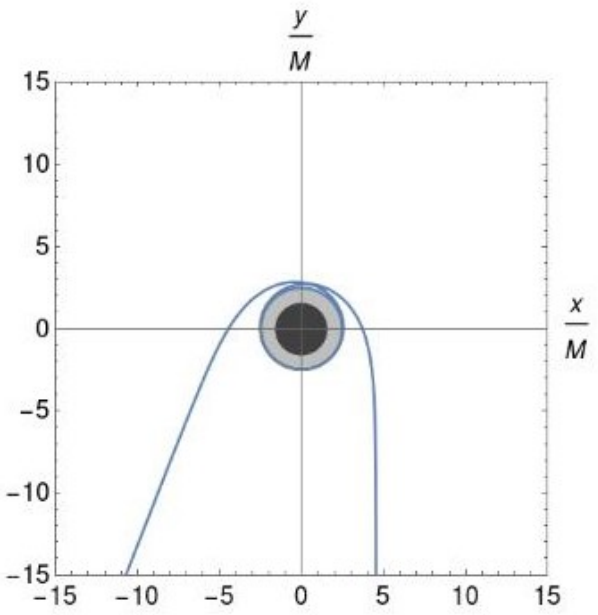

Figure 17: A photon path around a Reissner-Nordström black hole with an impact parameter that is equal to the critical impact parameter. The RN black hole has a charge of $Q = 0.8M$. The corresponding critical impact parameter is approximately $b_{\text{crit}} = 4.55M$. The photon enters the photon ring, however because of the instability of the photon ring in combination with numerical error, the photon also leaves the black hole and goes back into space.

4.6.1 Deflection of light by power expansion

We substitute the RN metric into Eq. (2.4.2). We get the differential equation

$$\frac{d^2u}{d\phi^2} + u = 3Mu^2 - 2Q^2u^3. \tag{4.6.1}$$

Yet again, we write u as an expansion in terms of Mu_0, see Eq. (2.4.3). We substitute this expansion into Eq. (4.4.1) and sort all terms with the same power of Mu_0. We get the equations

$$\frac{d^2u_1}{d\phi^2} + u_1 = 3\cos^2\phi, \tag{4.6.2}$$

$$\frac{d^2u_2}{d\phi^2} + u_2 = 6u_1\cos\phi - 2Q^2\cos^3\phi. \tag{4.6.3}$$

In these set of equations, we recognize Eq. (4.6.2) from chapter 3. The results of these equations are

$$u_1 = \frac{3 - \cos 2\phi}{2}, \tag{4.6.4}$$

$$u_2 = -\frac{3}{4}Q^2\phi\sin\phi + \frac{1}{16}Q^2\cos 3\phi + \frac{15}{4}\phi\sin\phi + \frac{3}{16}\cos 3\phi. \tag{4.6.5}$$

We substitute this result in Eq. (2.4.3) and we get

$$u = u_0(\cos\phi + Mu_o\frac{3-\cos 2\phi}{2} + (Mu_0)^2(-\frac{3}{4}Q^2\phi\sin\phi + \frac{1}{16}Q^2\cos 3\phi + \frac{15}{4}\phi\sin\phi + \frac{3}{16}\cos 3\phi)), \tag{4.6.6}$$

where $u_0 = 1/b$. We take the Taylor series of this value around u goes to zero (see figure 8). The result is

$$\theta = \frac{2M}{b} + \frac{3\pi}{8b^2}(5M^2 - Q^2), \tag{4.6.7}$$

which we have to multiply by two, because of the symmetry in the system. This gives the final result for the deflection angle in a Reissner-Nordström metric,

$$\delta\phi = \frac{4M}{b} + \frac{3\pi}{4b^2}(5M^2 - Q^2). \tag{4.6.8}$$

We see that the charge term only affects the sub-leading order of the deflection angle. This agrees with the fact that the charge term has an inverse quadratic dependency on the radius.

4.6.2 Gauss-Bonnet

When we substitute the RN metric in the expression for the Gauss-Bonnet theorem Eq. (2.4.5) and Eq. (2.4.6) we get

$$K = -(-\frac{1}{4}(\frac{2M}{r^2} - \frac{2Q^2}{r^3})^2 + \frac{1}{2}(-\frac{4M}{r^3} + \frac{6Q^2}{r^4})(1 - \frac{2M}{r} + \frac{Q^2}{r^2})) \tag{4.6.9}$$

and

$$dS = (1 - \frac{2M}{r} + \frac{Q^2}{r^2})^{-3/2})rdrd\phi. \tag{4.6.10}$$

Together this yields

$$KdS = -(1 - \frac{2M}{r} + \frac{Q^2}{r^2})^{-3/2}(\frac{2M}{r^2} - \frac{3}{r^3}(M^2 + Q^2) + \frac{6MQ^2}{r^4} - \frac{2Q^4}{r^5})drd\phi. \tag{4.6.11}$$

We now take the Taylor expansion of this expression for r goes to infinity and we get

$$KdS = -\frac{2M}{r^2} + \frac{3}{r^3}(Q^2 - M^2). \tag{4.6.12}$$

For the deflection angle we can now use Eq. (2.4.10) This gives

$$\delta\phi = -\int_{-1/2\pi}^{1/2\pi}\int_{u^{-1}}^{\infty} -\frac{2M}{r^2} + \frac{3}{r^3}(Q^2 - M^2)drd\phi, \tag{4.6.13}$$

where

$$u = \frac{\cos\phi}{b} + \frac{M}{b^2}\frac{3 - \cos 2\phi}{2}. \tag{4.6.14}$$

This is the same expression as for the Schwarschild spacetime in chapter 3, because the electromagnetic charge appears at higher order and we are only interested in the leading and sub-leading term of the deflection angle. Solving the integral in Eq. (4.6.13) gives

$$\delta\phi = \frac{4M}{b} + \frac{3\pi}{4b^2}(5M^2 - Q^2). \tag{4.6.15}$$

This is the same as Eq. (4.6.7). We can now plot the deflection angle in the photon path plot. In figure 18 we have plotted the deflection angle of a photon with impact parameter $b = 10$ for a black hole with charge $Q = 0.8M$. In the figure it looks like the Schwarzschild deflection angle is a better approximation of the photon path than the Reissner-Nordström deflection angle. We will explain why this is not the case.

It is difficult to test the effect of the charge term in the deflection angle. This is because photon paths with low impact parameters are affected by charge the most. Photon paths with high impact parameters are well approximated by the Schwarzschild case,

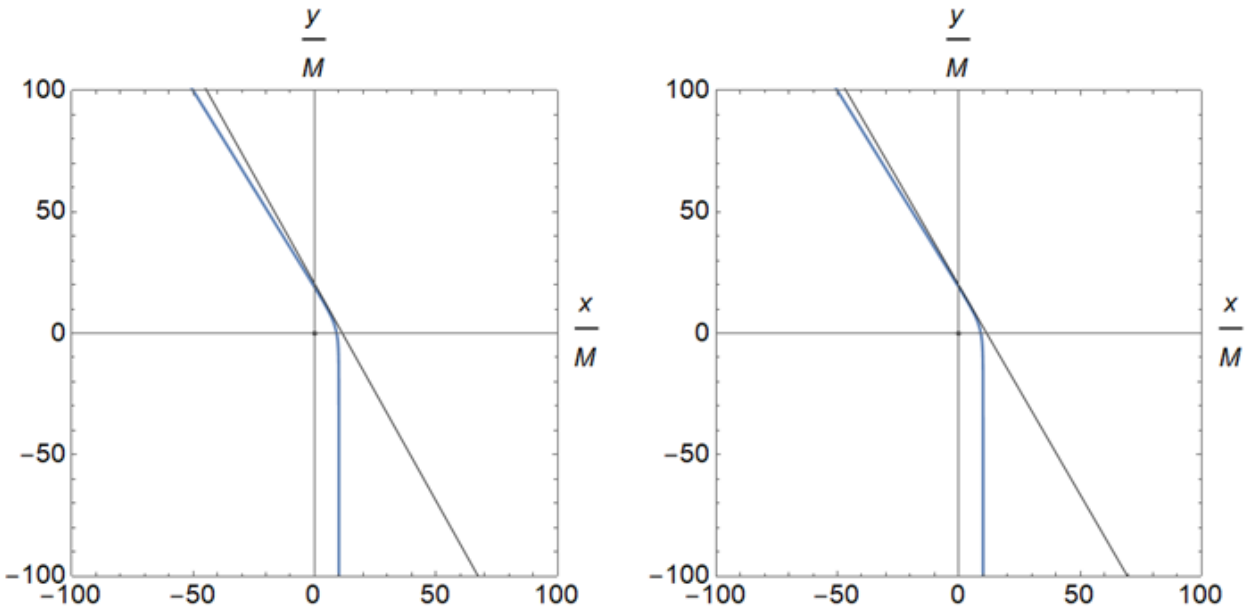

Figure 18: The deflection angle and the photon path around a Reissner-Nordström black hole with charge $Q = 0.8M$. The figure on the left side contains the Reissner-Nordström deflection angle and the figure on the right side contains the Schwarzschild deflection angle. For both graphs the linear and quadratic term have been taken into account.

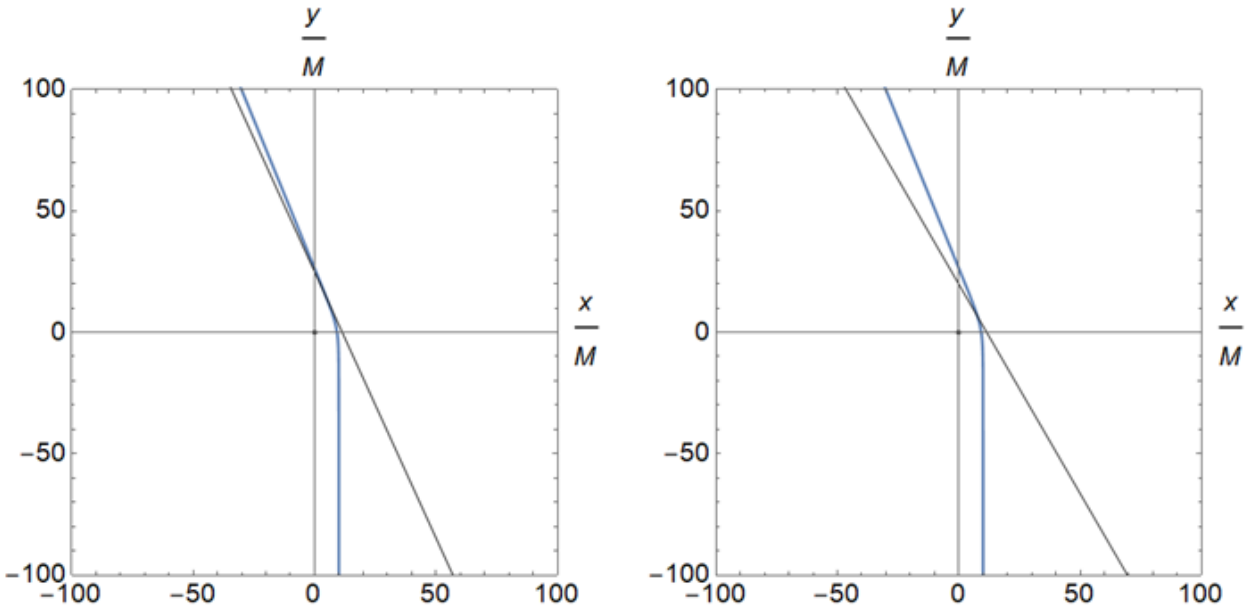

Figure 19: The deflection angle and the photon path around a Reissner-Nordström black hole with charge $Q = 2.0M$. The figure on the left side contains the Reissner-Nordström deflection angle and the figure on the right side contains the Schwarzschild deflection angle. For both graphs the linear and quadratic term have been taken into account.

because of the $1/r^2$ dependence on charge in the metric. However, in chapter 3 we have seen that the deviation from the photon path to the deflection angle for small impact parameters was large, because the higher order correction terms are more important in the deflection angle and we have only included the leading and sub-leading terms in M. Thus, the effect of the charge term on the deflection angle is larger for photons with a small impact parameter, but so are the higher order correction terms. Therefore it looks like the deflection angle for the Schwarzschild black hole is a better approximation to the Reissner-Nordström black hole than the actual RN deflection angle. However, the deviation in the deflection angle for low impact parameter photons (see figure 10) cancels the charge term and only make it seem like a better approximation.

To really check the deflection angle for the Reissner-Nordström case, we have to look at black holes with large values of Q compared to M, that is, naked singularities. In this case the effect of the charge term is significantly larger. In figure 19, we have plotted the photon path with impact parameter $b = 10M$ for a naked singularity with the charge $Q = 2.0M$. We now indeed see that the Reissner-Nordström deflection angle is a better approximation than the Schwarzschild result.

5 Einstein-scalar theory

5.1 Motivation

Now we turn to a modified gravitational theory, which is the Einstein-scalar theory. The Einstein-scalar theory still uses the Einstein equation, but couples it to a complex scalar field. The objects that arise from the Einstein-scalar theory are called boson stars. Boson stars are hypothetical objects. They are called black hole mimickers, because they can be very compact. They can not reach the level of compactness of a black hole, but they can be so compact that they look like one.

It would be very valuable to detect a boson star. On one hand boson stars are a dark matter candidate. This means that detecting them would tell us a lot about the origin of dark matter. On the other hand, when we detect a boson star it will most likely be made out of beyond the standard model particles. It can therefore help us extend the standard model of particle physics.

In this chapter we will calculate the photon paths around a boson star. To do this we first have to calculate the background solution. We can put the background solution in the equations of motion to find the photon paths.

5.2 Background solution

To derive the background solution for boson stars, we first need to solve the Einstein equation

$$G_{\mu\nu} = 8\pi T_{\mu\nu}. \tag{5.2.1}$$

In this equation the left side is the Einstein curvature tensor. This tensor describes the curvature of spacetime. On the right hand side of the Einstein equation we have the stress-energy tensor. In other words, the Einstein equation relates the curvature of space to the energy and momentum density. To calculate the Einstein curvature tensor, we use the general metric in spherical coordinates given by Eq. (2.1.1). We again assume that this metric is static and thus that the components of the metric do not depend on time. The components of the Einstein curvature tensor for this metric are

$$G_{tt} = \frac{A(r)}{r^2 B(r)^2}(rB'(r) - B(r) + B(r)^2), \tag{5.2.2a}$$

$$G_{rr} = \frac{1}{r^2}(\frac{rA'(r)}{A(r)} - B(r) + 1), \tag{5.2.2b}$$

$$G_{\theta\theta} = \frac{r^2}{4A(r)^2 B(r)^2}(-\frac{2B'(r)A(r)^2}{r} + \frac{2A'(r)A(r)B(r)}{r} + 2A''(r)A(r)B(r) - A'(r)B'(r)A(r) - A'(r)^2 B(r)), \tag{5.2.2c}$$

$$G_{\phi\phi} = \frac{r^2 \sin^2(\theta)}{4A(r)^2 B(r)^2}(-\frac{2B'(r)A(r)^2}{r} + \frac{2A'(r)A(r)B(r)}{r} + 2A''(r)A(r)B(r) - A'(r)B'(r)A(r) - A'(r)^2 B(r)). \tag{5.2.2d}$$

The metric in Eq. (2.1.1) does not have any cross-terms. Because the metric and the Einstein curvature tensor are directly related, the Einstein curvature tensor also does not have any cross-terms. Therefore we have to choose the complex scalar field such that the cross-terms of the stress-energy tensor vanish. For the stress-energy tensor [9] we have

$$T_{\mu\nu} = \frac{1}{2}(\nabla_\mu \bar{\psi} \nabla_\nu \psi + \nabla_\mu \psi \nabla_\nu \bar{\psi}) - \frac{1}{2} g_{\mu\nu}(g^{\lambda\rho} \nabla_\lambda \bar{\psi} \nabla_\rho \psi + 2V(|\psi|^2)), \tag{5.2.3}$$

In this equation ψ is the complex scalar field[1]. Because ψ is a (complex) scalar, the covariant derivatives can be replaced by partial derivatives. The diagonal terms of the stress-energy tensor are given by

$$T_{tt} = \frac{1}{2}(\partial_t \bar{\psi} \partial_t \psi + \partial_t \psi \partial_t \bar{\psi}) + \frac{1}{2} A(r)(g^{\lambda\rho} \partial_\lambda \bar{\psi} \partial_\rho \psi + 2V(|\psi|^2)), \tag{5.2.4a}$$

$$T_{rr} = \frac{1}{2}(\partial_r \bar{\psi} \partial_r \psi + \partial_r \psi \partial_r \bar{\psi}) - \frac{1}{2} B(r)(g^{\lambda\rho} \partial_\lambda \bar{\psi} \partial_\rho \psi + 2V(|\psi|^2)), \tag{5.2.4b}$$

$$T_{\theta\theta} = \frac{1}{2}(\partial_\theta \bar{\psi} \partial_\theta \psi + \partial_\theta \psi \partial_\theta \bar{\psi}) - \frac{r^2}{2}(g^{\lambda\rho} \partial_\lambda \bar{\psi} \partial_\rho \psi + 2V(|\psi|^2)), \tag{5.2.4c}$$

$$T_{\phi\phi} = \frac{1}{2}(\partial_\phi \bar{\psi} \partial_\phi \psi + \partial_\phi \psi \partial_\phi \bar{\psi}) - \frac{r^2}{2}(g^{\lambda\rho} \partial_\lambda \bar{\psi} \partial_\rho \psi + 2V(|\psi|^2)). \tag{5.2.4d}$$

In these expressions we have

$$g^{\lambda\rho} \nabla_\lambda \bar{\psi} \nabla_\rho \psi = -\frac{1}{A(r)} \partial_t \bar{\psi} \partial_t \psi + \frac{1}{B(r)} \partial_r \bar{\psi} \partial_r \psi + \frac{1}{r^2} \partial_\theta \bar{\psi} \partial_\theta \psi + \frac{1}{r^2 \sin^2 \theta} \partial_\phi \bar{\psi} \partial_\phi \psi. \tag{5.2.5}$$

To solve the Einstein equation we have to define the potential of the system. We assume a massive, free field case, meaning that the system does not interact with itself. The corresponding potential is

$$V(|\psi|^2) = \frac{1}{2} m^2 |\psi|^2 = \frac{1}{2} m^2 \psi \bar{\psi}. \tag{5.2.6}$$

[1]The scalar field is often written as ϕ, however in this thesis we write is as ψ to not confuse it with angle ϕ for spherical coordinates

The m in this equation is the bare mass of the system. Even though the Einstein curvature tensor is zero for all the off-diagonal terms, this is not the case for the stress-energy tensor. For the off-diagonal case we have

$$T_{\mu\nu} = \frac{1}{2}(\partial_\mu\bar{\psi}\partial_\nu\psi + \partial_\mu\psi\partial_\nu\bar{\psi}), \tag{5.2.7}$$

Where $\mu \neq \nu$. Because of the Einstein equation, all these off-diagonal terms have to be equal to zero. As said before, this means that the scalar function has to be chosen in such a way that the off-diagonal terms vanish. We are only interested in spherically symmetric systems. We can hence take a spherically symmetric scalar field and we define the the scalar field such that it only depends on the radius r and the time t. We take the simplest relation between the radial and time part of the scalar field

$$\psi = \psi(r)e^{i\omega t}. \tag{5.2.8}$$

This relation indeed causes all the off-diagonal terms of the stress-energy tensor to vanish. Because the scalar function only depends on r and t, the partial derivatives of the scalar function with respect to ϕ and θ will vanish. Furthermore, we assume that the system is spherically symmetric. This means we can choose the angle θ and we set this, just like before, at $\theta = \pi/2$. The Einstein equation in the different directions becomes.

Time direction:

$$\frac{A(r)}{r^2B(r)^2}(rB'(r) - B(r) + B(r)^2) = 4\pi(\psi(r)^2\omega^2 + \frac{A(r)}{B(r)}\psi'(r)^2 + 2V(|\psi|^2)A(r)). \tag{5.2.9}$$

Radial direction:

$$\frac{1}{r^2}(r\frac{A'(r)}{A(r)} - B(r) + 1) = 4\pi(\psi'(r)^2 + \frac{B(r)}{A(r)}\psi(r)^2\omega^2 - 2B(r)V(|\psi|^2)). \tag{5.2.10}$$

θ direction:

$$\begin{aligned}&\frac{1}{4A(r)B(r)}(-\frac{2B'(r)A(r)^2}{r} + \frac{2A'(r)A(r)B(r)}{r} + 2A''(r)A(r)B(r) - A'(r)B'(r)A(r)\\ &-A'(r)^2B(r)) = -4\pi(-B(r)\psi(r)^2\omega^2 + A(r)\psi'(r)^2 + 2A(r)B(r)V(|\psi|^2)).\end{aligned} \tag{5.2.11}$$

Because of the spherical symmetry, the $\sin\theta$ terms in the ϕ direction vanish and the Einstein equation for the ϕ direction equals the one in the θ direction. We see that the scalar function, and thus the matter distribution, depends on the time t. However, the final Einstein equation does not. This is because the scalar function never appears in the stress-energy tensor alone, but only in pairs with its complex conjugate. Therefore the time dependence disappears in the final Einstein equations. This is a crucial result, because we assumed the metric is not time dependent. So even though the matter distribution is time dependent, the curvature of space caused by this matter distribution

is not.

To solve the system of differential equations, we also use the Klein-Gordon equation. The Klein-Gordon equation for a scalar field ψ is given by

$$g^{\mu\nu}\nabla_\mu\nabla_\nu\psi = 2\frac{dV}{d|\psi|^2}\psi, \tag{5.2.12}$$

with the quantity

$$\nabla_\mu\nabla_\nu\psi = \partial_\mu\partial_\nu\psi - \partial_\lambda\psi\Gamma^\lambda_{\mu\nu}. \tag{5.2.13}$$

Substituting this equation into the general metric gives the equation

$$\begin{aligned}&\frac{1}{A(r)}(\psi(r)e^{i\omega t}\omega^2 + \frac{1}{2}\psi'(r)e^{i\omega t}\frac{A'(r)}{B(r)}) + \frac{1}{B(r)}(\psi''(r)e^{i\omega t} - \frac{1}{2}\psi'(r)e^{i\omega t}\frac{B'(r)}{B(r)})\\ &+ \frac{2}{rB(r)}\psi'(r)e^{i\omega t} = m^2\psi.\end{aligned} \tag{5.2.14}$$

Combining Eq. (5.2.13) with the system of equations in the different directions gives the final system of background equations

$$A'(r) = 4\pi rA(r)(\psi'(r)^2 + B(r)\psi(r)^2\frac{\omega^2}{A(r)} - B(r)\psi(r)^2) + \frac{B(r)A(r)}{r} - \frac{A(r)}{r}, \tag{5.2.15a}$$

$$B'(r) = 4\pi rB(r)^2(\psi(r)^2\frac{\omega^2}{A(r)} + \frac{\psi'(r)^2}{B(r)} + m^2\psi(r)^2) + \frac{B(r)}{r} - \frac{B(r)^2}{r}, \tag{5.2.15b}$$

$$\psi''(r) = B(r)\psi(r)(1 - \frac{\omega^2}{A(r)}) - \frac{1}{2}\psi'(r)\frac{A'(r)}{A(r)} + \frac{1}{2}\psi'(r)\frac{B'(r)}{B(r)} - \frac{2}{r}\psi'(r). \tag{5.2.15c}$$

The final background system consists of only three equations, even though we have found four of them. However, Eq. (5.2.11) can be derived from the final background system. That is why we do not include that equation in the final system. To solve the background system we set $m = 1$.

5.3 Numerical methods

To solve the system in Eq. (5.2.14) we first have to define a number of boundary conditions. The boundary conditions we use are

$$\psi(0) = \psi_c, \tag{5.3.1a}$$

$$\psi'(0) = 0, \tag{5.3.1b}$$

$$B(0) = 1, \tag{5.3.1c}$$

$$\lim_{r\to\infty}\psi(r) = 0, \tag{5.3.1d}$$

$$\lim_{r\to\infty}A(r) = \lim_{r\to\infty}\frac{1}{B(r)}. \tag{5.3.1e}$$

The first three conditions guarantee regularity at the origin. The last two equations guarantee flatness of spacetime for infinite distance from the boson star. The system in Eq. (5.2.15) can not be solved numerically for the set of boundary conditions in Eq. (5.3.1) in a direct way. We have to use some tricks to solve this system. The first trick we used is spatial compactification [10]. This means that we transform the domain of r with a function from $[0, \infty)$ to $[0, 1)$. This makes it easier to look at the behaviour of the background solution at larger distances. To do this, we use the transformation

$$\zeta(r) = \frac{r}{r_0 + r}. \tag{5.3.2}$$

In this transformation r_0 is the point $\zeta(r_0) = 1/2$. $\zeta(r)$ is the transformed distance coordinate. We chose $r_0 = 30M$, but any distance can be used as long as the distance is high enough to assume flatness.

The next trick that we used to solve the background equations for the first four boundary conditions numerically is the shooting method. This changes the boundary value problem to an initial value problem. Instead of implementing Eq. (5.3.1d), we specified a particular value for ψ_c and solved this system for different values of ω. We search for an ω afterwards for which boundary condition Eq. (5.3.1d) is satisfied. What can be observed is that this boundary condition is satisfied for more than one value of ω, however we would like to use the ground state, which is the function for ψ that does not cross the zero point for ψ. Figure 20 shows two function for ψ for which the boundary condition is satisfied. However, for only one of those two the system is in the ground state.

After we have found a value of ω for which boundary condition Eq. (5.3.1d) is satisfied and the system is in the ground state, we are still left with boundary condition Eq. (5.3.1e). From Eq. (5.2.15), it is clear that $A(r)$ always appears in combination with ω^{-2} or with the inverse of the derivative of $A(r)$. Consequently, multiplying $A(r)$ and ω^2 with the same constant factor will not change the system of differential equations. Thus, we can multiply the intermediate solution for $A(r)$ and ω by a constant factor such that boundary condition in Eq. (5.3.1e) is satisfied. Now the system satisfies all the boundary conditions.

5.4 Results of the background solution

We will now look at some results of the background solution to get a better idea of how boson stars with different values of ψ_c look like. Figure 21 shows the scalar field ψ for different values of ψ_c. This figure shows that boson stars do not have a surface, in the sense that there is not a particular sphere containing all the mass of the boson star where the external pressure of the boson star disappears. That is why the radius of a boson star is mostly defined as the radius of the sphere that contains a certain percentage of the mass (i.e 95 or 99%). What can also be concluded from figure 21 is that the slope of the scalar field is steeper near the origin for higher values of ψ_c, so that the radius of the boson star decreases for higher values of ψ_c. We will now take a look at the mass of the boson stars. With the mass we mean the ADM mass. This is

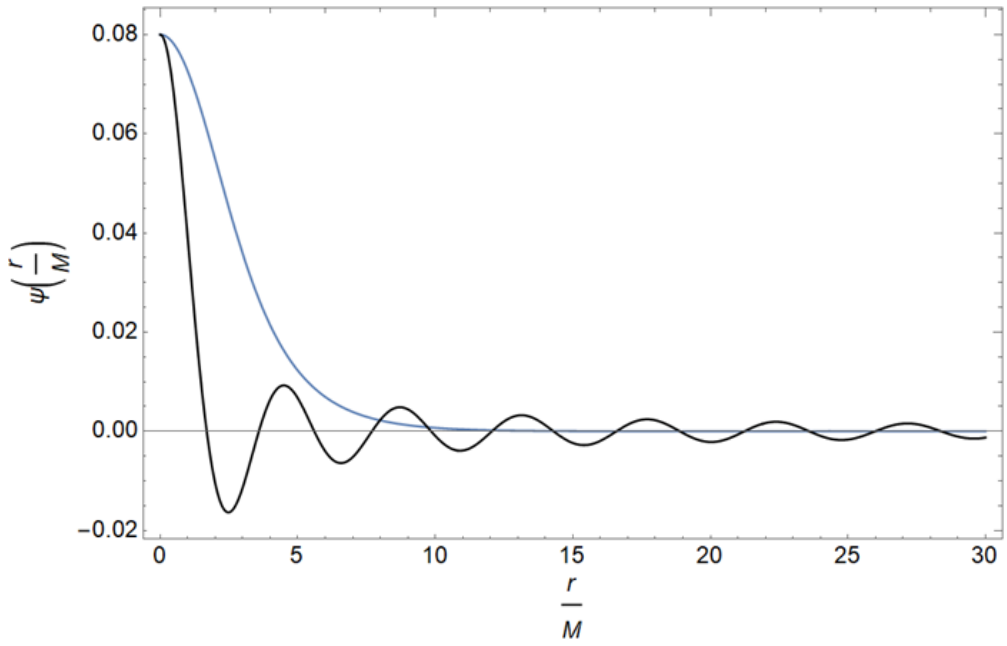

Figure 20: The function of ψ for $\psi_c = 0.08$. The black line is the ψ-function for $\omega = 1.52$. The ω for the blue line has a value of 0.85409, which we found to be the correct value of ω in our system for this particular value of ψ_c. Both functions satisfy the fourth boundary condition, however the function given by the blue line is in the ground state and the function given by the black line is in an excited state. The ψ function is transformed back to a function of r.

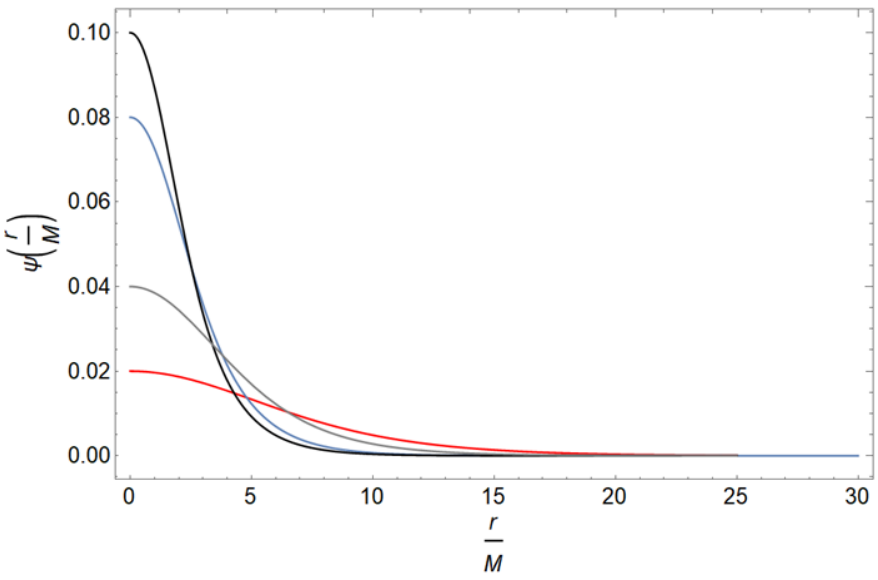

Figure 21: The scalar field function for different values of ψ_c as function of the distance r. The values of ψ_c are the scalar field values at the point $r = 0$. The scalar field function is steeper for higher values of ψ.

the gravitational pull the boson star will have on an object far away. The ADM mass can be calculated by rewriting

$$B(r) = \left(1 - \frac{2M_{ADM}}{r}\right)^{-1} \tag{5.4.1}$$

to an expression for M_{ADM} as a function of $B(r)$. The results are plotted in figure 22. We see that the ADM mass has a maximum around $\psi_c = 0.08$. The mass that corresponds to that peak is around $M_{ADM} = 0.63M$. For higher values of ψ_c the ADM mass gets constant. When we combine this result with figure 21, we see that a boson star with peak value $\psi_c = 0.08$ has a relatively high compactness (the compactness is calculated by dividing the mass of the star by its radius). Moreover, the compactness for boson stars gets higher for higher values of ψ_c, because of the decreasing radius and constant mass.

5.5 Photon paths

We have plotted the photon paths around boson stars for different values of ψ_c. Figure 23 shows the photon paths around a boson star with $\psi_c = 0.02$. From figure 22, we see that the mass of this boson star is very small, which is the reason of the weak gravitational effect on the null geodesics around the boson star. In figure 24 we have plotted the photon paths around a boson star with $\psi_c = 0.08$. we see that the corresponding mass of this boson star is relatively high, meaning that the gravitational pull on the surroundings is higher.

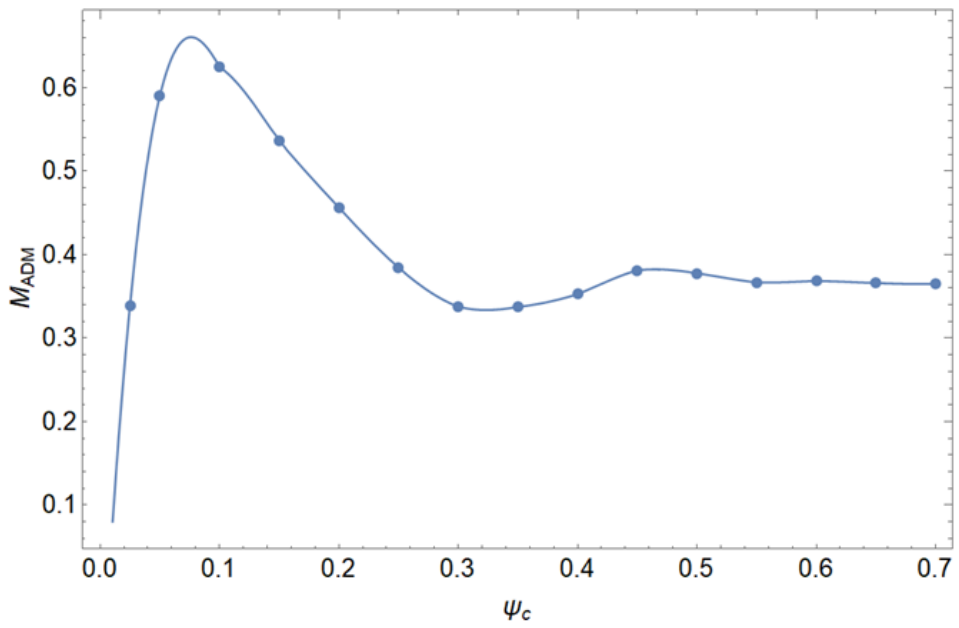

Figure 22: The ADM mass of boson stars for different values of ψ_c. There is a peak at $\psi_c = 0.08$. The mass of this boson star is around $M_{ADM} = 0.63M$. The ADM mass gets constant for high values of ψ_c.

5.6 Comparison of boson stars and Schwarzschild black holes

As we said at the beginning of the chapter, boson stars are black hole mimickers. We will now compare the boson star case with the Schwarzschild black hole case to check whether a boson star and a black hole with the same mass can look similar. To do this we used the boson star with the highest mass, because that would be the best approximation of a black hole. The boson star with the highest mass has $\psi_c = 0.08$ and has a mass of $M_{ADM} = 0.63M$. We have seen this boson star in figure 24. Figure 25 shows the Schwarzschild black hole with the same mass of $M_{ADM} = 0.63M$.

The most noticeable difference between these two plots are the low impact parameter photons. For the schwarzschild case the photons will fall into the black hole. However, given that the boson star does not have a horizon, photons are not absorbed and instead are deflected with a relatively high deflection angle. The high impact parameter photons look similar in both cases. In figure 27 we have plotted the photon paths with high impact parameter for both the Schwarzschild black hole and the boson star. We see that the black hole and the mimicker look indeed very similar for high impact parameter photons. The main difference between a black hole and a boson star with the same mass are the photon paths with a small impact parameter that are either absorbed or reflected with a high deflection angle.

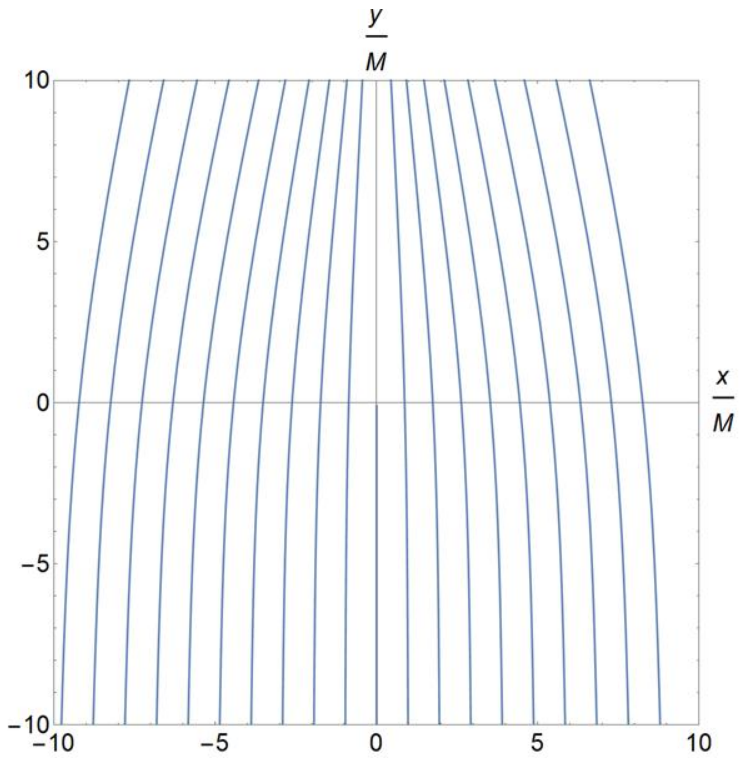

Figure 23: The photon paths around a boson star with $\psi_c = 0.02$. The mass of the boson star is around $M_{ADM} = 0.15M$. Because of the low mass of the boson star, the gravitational field is not affected much. Therefore the photon paths are not curved as much as in a black hole case.

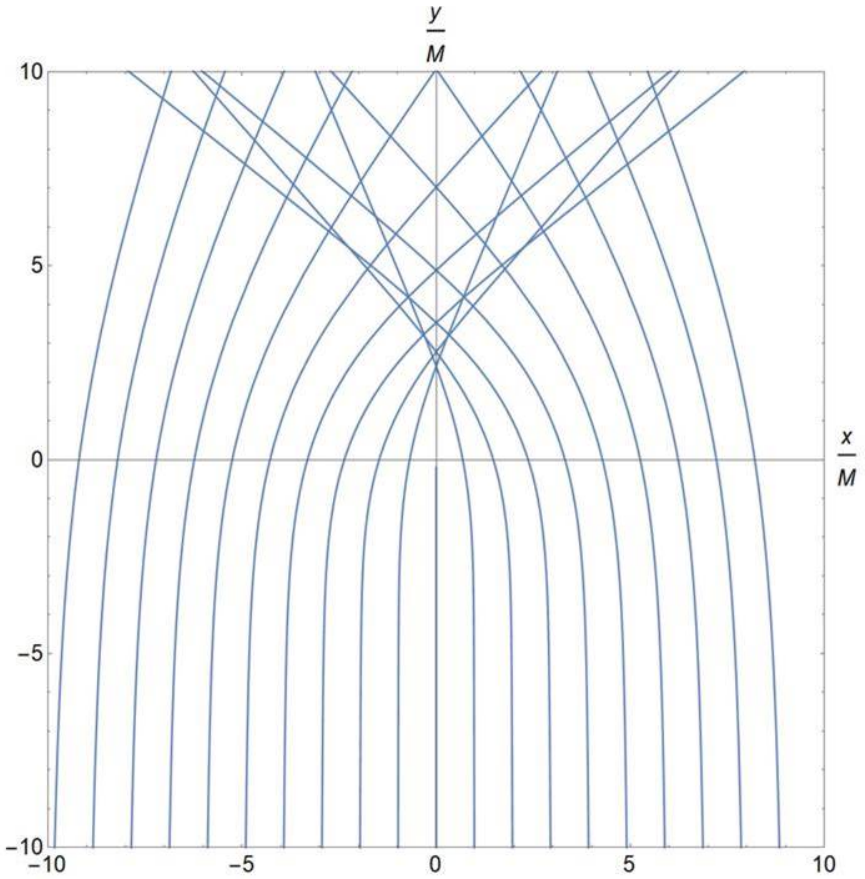

Figure 24: The photon paths around a boson star with $\psi_c = 0.08$, which has a mass of $M_{ADM} = 0.63M$. This is the boson star with maximal mass and thus the strongest gravitational pull.

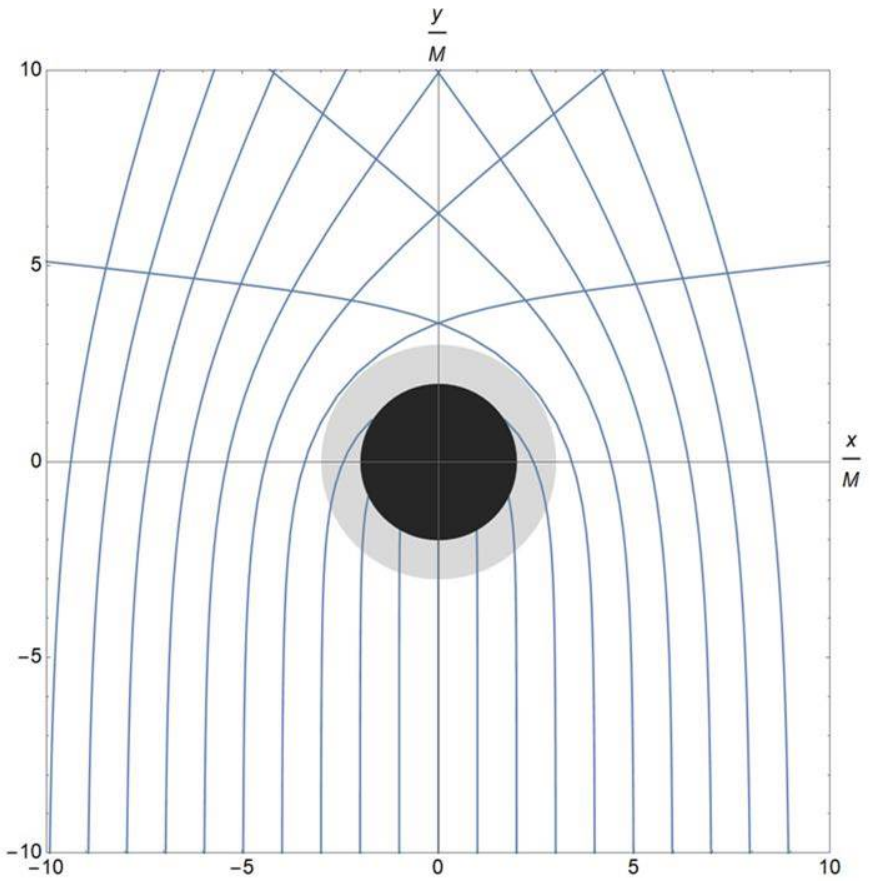

Figure 25: A Schwarzschild black hole with mass set to $0.63M$. It therefore has the same mass as the heaviest boson star. The black disc indicates the event horizon and the gray disc the photon ring.

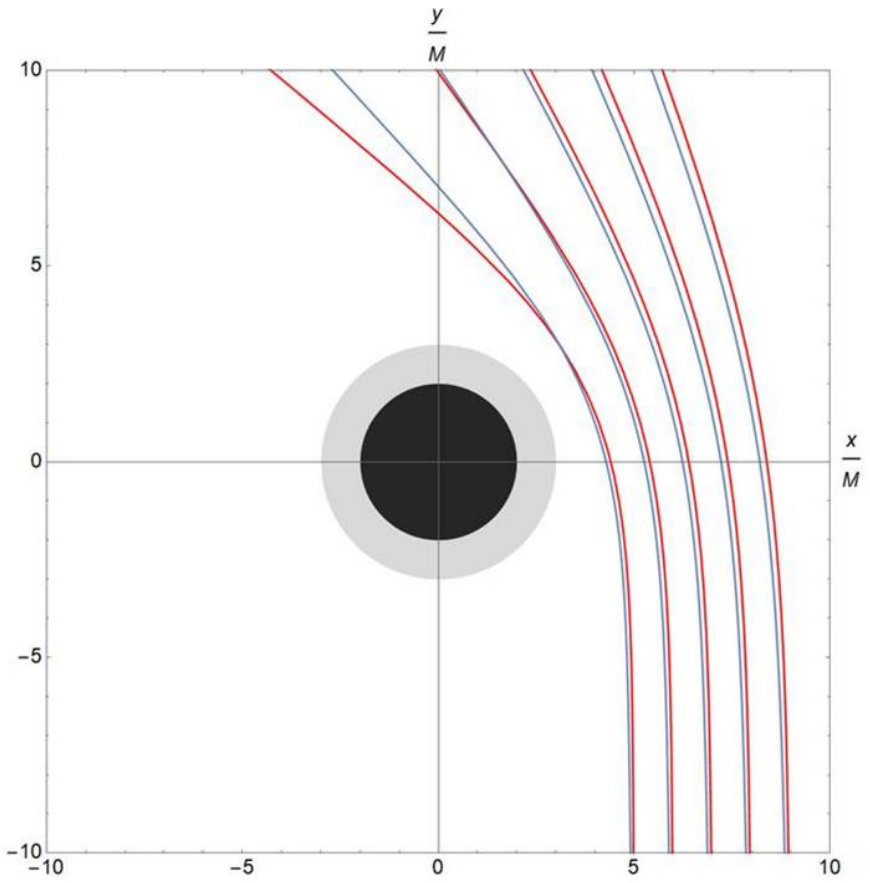

Figure 26: The photon paths around a Schwarzschild black hole and a boson star both with mass $0.63M$. The red lines indicate the photon paths around the Schwarzschild black hole and the blue lines around the boson star. The black and gray disc are shown as reference point for the photon paths, but are not there in the boson star case.

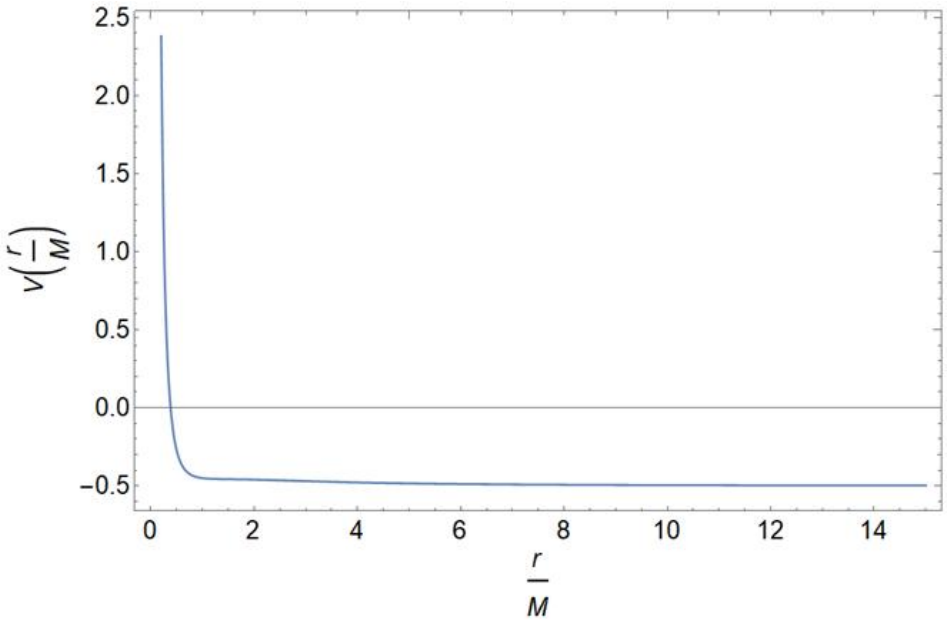

Figure 27: The effective potential plot for a boson star with $\psi_c = 0.7$ as function of the distance. Because there are no extreme values visible in this plot, there are no circular orbits around this boson star.

5.7 Circular orbits and deflection angle

We would now like to know whether a boson star can have circular orbits around them. We can determine if a boson star has circular orbits by examining the effective potential function in Eq. (2.2.2). The boson star type that has the most chance of having a circular orbit is the type of boson stars that have a high mass and a high compactness. This means we can check the effective potential function for this type of boson star to see if there are any extreme values. We use the boson star where $\psi_c = 0.7$. The boson star with $\psi_c = 0.08$ is less suitable, because the radius is too big. The smaller the radius of a Boson star, the higher the deflection angle of a photon with a certain impact parameter. In figure 27 we have plotted the effective potential function for the boson star with $\psi_c = 0.7$. There are no extreme values in this potential plot. This means that there are no photon rings around a boson star.

It is also possible to calculate the deflection angle of the boson stars by solving Eq. (2.4.2) or by using the Gauss-Bonnet theorem, however we leave that for further research.

6 Conclusion and Discussion

In this thesis, we described a framework that can be used to calculate photon paths and their properties around black holes and black hole mimickers. We calculated the equations of motion of the photon paths by using Killing vectors. Other properties we looked at are the circular orbits around a black hole for massless as well as for massive particles, the critical impact parameter and the deflection angle. The photon paths and their properties can be helpful when one wishes to analyze and predict the nature of compact objects.

In later chapters, we applied the framework in chapter 2 to different types of black holes and black hole mimickers. We first did this for a Schwarzschild black hole in chapter 3. Because Schwarzschild black holes are relatively simple, there is a lot already known about this type of black hole and we could compare our results with earlier research. All our results agree with the established literature. For instance, our results in figure 6 agree with [11]. Therefore, we gained confidence that the expressions in chapter 2 for general spherically symmetric spacetimes are correct.

In chapter 4 we applied the expressions from chapter 2 to the Reissner-Nordström metric, which is an extension of the Schwarzschild metric. We were not able to find a source which plotted the photon paths in a Reissner-Nordström metric, however, general properties of null geodesics near these charged black holes are also well-known and agree with our results. For instance, the fact that RN black holes have no horizon for $Q > M$, that these types of black holes are repellent [8] and the expression for the deflection angle [12] and critical impact parameter [13].

After looking at these two black hole solutions, we applied our framework to a modified theory of gravity, which is the Einstein-scalar theory. This theory couples the Einstein curvature tensor to a (complex) scalar field. To apply the expressions in chapter 2 to the modified gravitational theory we first had to calculate the background solution, i.e., the equivalent of the black hole solution in this modified gravitational theory. In fact, we did not consider a black hole type solution, but a black hole mimicker known as a boson star. There are no analytic solutions known, so we resorted to numerical methods to describe these boson stars. After calculating the background solution, it is relatively simple to study its properties and null geodesics using the framework of chapter 2. We plotted the photon paths for different boson stars characterized by different scalar field and different charges. To easily compare, in figure 26 we plotted both the photon paths around a Schwarzschild black hole and a boson star. We can conclude from figure 26 that it is hard to distinguish a Schwarzschild black hole from a boson star with the same mass. Distinguishing these two objects can be done by measuring highly deflected photons coming from photon paths with low impact parameters. For the Einstein-scalar theory we leave the calculation of the deflection angle and the ISCO for future research. These properties can be calculated with the help of the expressions in chapter 2. These expressions can also be applied to other spherically symmetric objects in other modified gravitational theories, such as the Einstein-Maxwell-scalar

(EMS) theory. The calculations of the background spacetime of the EMS theory are included in the Appendix.

As we said in the introduction, the results in this thesis can not be related to real-world observations. We, on one hand, assumed spherical symmetry in the system. This is not the case for most of the black holes. Consequently, we actually have to use the Kerr metric instead of the Schwarzschild metric, which allows angular momentum and does not preserve spherical symmetry. The framework in chapter 2 can not be used on a metric that does not preserve spherical symmetry. On the other hand, we assumed that the photons were coming from right behind the black hole, which is also not the case in real-world observations. In most cases the photons are coming from the accretion disc. Predicting photon paths coming out of the accretion disc is more difficult, because this means that we are not working in a vacuum region anymore. Taking matter into account would drastically increase the number of free parameters. Therefore, predicting these photon paths can not be done analytically and requires modelling with high-end code runs to keep track of every interaction in the system.

References

[1] S. Chandrasekhar. *Shakespeare, Newton, and Beethoven*. 1975, Ryerson Lecture, University of Chicago

[2] *Astronomers Capture First Image of a Black Hole*. https://eventhorizontelescope.org/press-release-april-10-2019-astronomers-capture-first-image-black-hole

[3] G.S. Bisnovatyi-Kogan, O.Yu. Tsupko, V. Perlick. *Shadow of black holes at local and cosmological distances*. 2019. ArXiv: 1910.10514v1

[4] Emanuele Berti. *A Black-Hole Primer: Particles, Waves, Critical Phenomena and Superradiant Instabilities*. Bad Honnef School, 2014. ArXiv: 1410.4481

[5] Jeremiah Bodenner, Clifford M. Will. *Deflection of light to second order: A tool for illustrating principles of general relativity*. 2003.

[6] G. W. Gibbons, M. C. Werner. *Applications of the Gauss-Bonnet theorem to gravitational lensing*. University of Cambridge, 2008. ArXiv: 0807.0854v1

[7] G. W. Gibbons, M. Vyska. *The application of Weierstrass elliptic functions to Schwarzschild null geodesics*. 2012.

[8] Sean M. Carroll. *Lecture Notes on General Relativity*. University of California, 1997. ArXiv: gr-qc/9712019v1

[9] Steven L. Liebling, Carlos Palenzuela. *Dynamical Boson Stars*. 2017. ArXiv: 1202.5809v3

[10] Chi Wai (Kevin) Lai. *A Numerical Study of Boson Stars*. The Chinese University of Hong Kong, 2004. ArXiv: 0410040v2

[11] *Black Hole Shadow*. https://odysseyedu.wordpress.com/black-hole-shadow/

[12] Jop Briët, David W. Hobill. *Gravitational Lensing by Charged Black Holes*. University of Calgary, Calgary, Alberta, Canada.

[13] Rogério Augusto Capobianco. *Geodesic motion in the Reissner-Nordström spacetime*. 2019.

[14] Shahar Hod. *Spontaneous scalarization of charged Reissner-Nordström black holes: Analytic treatment along the existence line*. Israel, 2020. ArXiv:2002.01948v1

[15] D. Astefanesei, C. Herdeiro, A. Pombo and E. Radu. *Einstein-Maxwell-scalar black holes: classes of solutions, dyons and extremality*. 2019. ArXiv:1905.08304

[16] Jose Luis Blazquez-Salcedo, Carlos A. R. Herdeiro, Jutta Kunz, Alexandre M. Pombo. and Eugen Radu. *Einstein-Maxwell-scalar black holes: the hot, the cold and the bald*. 2020. ArXiv:2002.00963

[17] Andrew Sullivan, Nicol as Yunes, and Thomas P. Sotiriou. *Exact Black Hole Solutions in Modified Gravity Theories: Spherical Symmetry Case*. 2019. ArXiv:1903.02624v1

[18] Andrew Sullivan, Nicol as Yunes, and Thomas P. Sotiriou. *Black Hole Shadows, Photon Rings, and Lensing Rings*. 2019. ArXiv:1906.00873v2

[19] David Garfinkle, Gary T. Horowitz, Andrew Strominger. *Charged black holes in string theory* . University of California, 1990.

[20] S. Chandrasekhar *The Mathematical Theory of Black Holes*. 1998.

A Equations of motion with the geodesic equation

In chapter 2 we found equations of motion for photons in a general spherically symmetric system. We can check these equations by using the geodesic equation

$$\frac{d^2x^\mu}{d\lambda^2} + \Gamma^\mu_{\alpha\beta}\frac{dx^\alpha}{d\lambda}\frac{dx^\beta}{d\lambda} = 0, \tag{A.1}$$

in which the Christoffel symbols are defined by

$$\Gamma^\mu_{\alpha\beta} = \frac{1}{2}g^{\mu\gamma}(g_{\gamma\alpha,\beta} + g_{\gamma\beta,\alpha} - g_{\alpha\beta,\gamma}) \tag{A.2}$$

with

$$g_{\alpha\beta,\gamma} = \frac{\partial g_{\alpha\beta}}{\partial x^\gamma}. \tag{A.3}$$

The Christoffel symbols are symmetric in α and β. The non-vanishing Christoffel symbols of the general metric in Eq. (2.1.1) take the form

$$\Gamma^t_{tr} = \Gamma^t_{rt} = \frac{1}{2}\frac{A'(r)}{A(r)}, \tag{A.4a}$$

$$\Gamma^r_{tt} = \frac{1}{2}\frac{A'(r)}{B(r)}, \tag{A.4b}$$

$$\Gamma^r_{rr} = \frac{1}{2}\frac{B'(r)}{B(r)}, \tag{A.4c}$$

$$\Gamma^r_{\theta\theta} = -\frac{r}{B(r)}, \tag{A.4d}$$

$$\Gamma^r_{\phi\phi} = -\frac{r\sin^2\theta}{B(r)}, \tag{A.4e}$$

$$\Gamma^\theta_{\phi\phi} = -\sin\theta\cos\theta, \tag{A.4f}$$

$$\Gamma^\theta_{\theta r} = \Gamma^\theta_{r\theta} = \frac{1}{r}, \tag{A.4g}$$

$$\Gamma^\phi_{\phi r} = \Gamma^\phi_{r\phi} = \frac{1}{r}, \tag{A.4h}$$

$$\Gamma^\phi_{\phi\theta} = \Gamma^\phi_{\theta\phi} = \frac{\cos\theta}{\sin\theta}. \tag{A.4i}$$

With these christoffel symbols, we can now derive the four components of the geodesic equation in Eq. (A.1). These are given by

$$\ddot{t} + \frac{A'(r)}{A(r)}\dot{t}\dot{r} = 0, \tag{A.5a}$$

$$\ddot{\theta} + \frac{2}{r}\dot{\theta}\dot{r} - \sin\theta\cos\theta\dot{\phi}^2 = 0, \tag{A.5b}$$

$$\ddot{\phi} + \frac{2}{r}\dot{\phi}\dot{r} + 2\frac{\cos\theta}{\sin\theta}\dot{\theta}\dot{\phi} = 0, \tag{A.5c}$$

$$\ddot{r} + \frac{1}{2}\frac{A'(r)}{B(r)}\dot{t}^2 - \frac{1}{2}\frac{B'(r)}{B(r)}\dot{r}^2 - \frac{r}{B(r)}(\dot{\theta}^2 + \dot{\phi}^2\sin^2\theta) = 0, \tag{A.5d}$$

with the dot denoting a derivative along the affine parameter λ. We now use the spherical symmetry of the system to set $\theta = \pi/2$ and thus $\dot{\theta} = \ddot{\theta} = 0$. The equations then simplify to

$$\ddot{t} + \frac{A'(r)}{A(r)}\dot{t}\dot{r} = 0, \tag{A.6a}$$

$$\ddot{\phi} + \frac{2}{r}\dot{\phi}\dot{r} = 0, \tag{A.6b}$$

$$\ddot{r} + \frac{1}{2}\frac{A'(r)}{B(r)}\dot{t}^2 - \frac{1}{2}\frac{B'(r)}{B(r)}\dot{r}^2 - \frac{r}{B(r)}\dot{\phi}^2 = 0. \tag{A.6c}$$

Taking the derivative of Eq. (2.1.5) gives Eq. (A.6a). This means that Eq. (A.6a) is the derivative of the time-component in the equations of motion in Eq. (2.1.16a). We can do the same for Eq. (2.1.6) and we obtain Eq. (A.6b). Thus, the derivative with respect to λ of Eq. (A.6b) corresponds to the angular component of the equations of motion. We will now show that Eq. (A.6c) corresponds to Eq. (2.1.9) for photons. Taking the derivative of Eq. (2.1.9) gives

$$2\dot{r}\ddot{r} = -\frac{E^2\dot{r}}{A(r)B(r)}\left(\frac{A'(r)}{A(r)} + \frac{B'(r)}{B(r)}\right) + \frac{L^2\dot{r}}{r^3B(r)^2}(2B(r) + rB'(r)), \tag{A.7}$$

which can be rewritten as

$$\ddot{r} = -\frac{E^2A'(r)}{2A(r)^2B(r)} + \frac{L^2}{r^3B(r)} - \frac{B'(r)}{2B(r)}\left(\frac{E^2}{A(r)B(r)} - \frac{L^2}{r^2B(r)}\right). \tag{A.8}$$

When we now substitute Eq. (2.1.9), Eq. (2.1.5) and Eq. (2.1.6) into Eq. (A.8), we get

$$\ddot{r} = -\frac{1}{2}\frac{A'(r)}{B(r)}\dot{t}^2 + \frac{1}{2}\frac{B'(r)}{B(r)}\dot{r}^2 + \frac{r}{B(r)}\dot{\phi}^2, \tag{A.9}$$

which is the same as Eq. (A.6c). Hence, we have now shown that the four components of the geodesic equation for the metric Eq. (2.1.1) are equal to the equations of motion.

B Einstein-Maxwell-scalar theory

Another modified gravitational theory, besides Einstein-scalar theory, is Einstein-Maxwell-Scalar (EMS) theory. In this modified gravitational theory the Einstein equation is not only coupled to a scalar field, but also to the Maxwell invariant. There are solutions for compact objects in EMS theory with event horizons and these solutions are therefore black holes. Black holes in the EMS theory have "hair", which means that they can not only be described by the charge, mass and angular momentum. So black holes with hair also depend on other factors, in this case the coupling between the scalar field and the Maxwell field.

B.1 Background solution

We will derive the background solution of the EMS theory. We leave the study of null geodesics of this background solution for further research. The action in the EMS theory [15] is given by

$$S = \frac{1}{16\pi}\int d^4x\sqrt{-g}(R - 2\partial_\mu\psi\partial^\mu\psi - f(\psi)F_{\mu\nu}F^{\mu\nu}). \tag{B.1}$$

The R in this equation is the Ricci scalar, ψ is the scalar field. We now use a real scalar field instead of a complex one. $f(\psi)$ is the coupling function between the scalar field and the Maxwell invariant. F is the Maxwell field. For the Maxwell field we have

$$F_{\mu\nu} = \partial_\mu A_\nu - \partial_\nu A_\mu. \tag{B.2}$$

This means that the Maxwell field is anti-symmetric. When we vary the action, the Einstein equation we find is

$$G_{\mu\nu} = 2\Big[\partial_\mu\psi\partial_\mu\psi - \frac{1}{2}g_{\mu\nu}\partial_\rho\psi\partial^\rho\psi + f(\psi)\Big(F_{\mu\rho}F^\rho_\nu - \frac{1}{4}g_{\mu\nu}F_{\rho\sigma}F^{\rho\sigma}\Big)\Big]. \tag{B.3}$$

For the Maxwell invariant we have

$$A_\mu = (V(r), \mathbf{A}), \tag{B.4}$$

in which $V(r)$ is the electric potential and $\mathbf{A}$ the magnetic vector potential. Just as we did for the Reissner-Nordström spacetime, we assume that the magnetic charge of the background solution we are after is zero. This means that only the time component of the Maxwell invariant will be non-zero. The only non-zero term of the Maxwell field is the term that combines the radius and time component, because the Maxwell invariant is only dependent on the radius in its time component. This means that the only non-zero terms will be

$$F_{rt} = -F_{tr} = V'(r). \tag{B.5}$$

We assume that the scalar function is real and does not depend on time such that

$$\psi = \psi(r). \tag{B.6}$$

For the Einstein curvature tensor we can use Eq. (5.2.2), because we are working with the same metric and the Einstein curvature tensor only depends on the spacetime metric. The Einstein equation for the different components becomes
Time direction:

$$\frac{A(r)B'(r)}{rB(r)} - \frac{A(r)}{r^2} + \frac{A(r)B(r)}{r^2} = A(r)\psi'(r)^2 + f(\psi)V'(r)^2. \tag{B.7}$$

Radius direction:

$$\frac{A'(r)}{r} + \frac{A(r)}{r^2} - \frac{B(r)A(r)}{r^2} = A(r)\psi'(r)^2 - f(\psi)V'(r)^2. \tag{B.8}$$

θ direction:

$$-\frac{A(r)B'(r)}{2rB(r)} + \frac{A'(r)}{2r} + \frac{A''(r)}{2} - \frac{A'(r)B'(r)}{4B(r)} - \frac{A'(r)^2}{4A(r)} = -A(r)\psi'(r)^2 + f(\psi)V'(r)^2. \tag{B.9}$$

To solve the background system we also use the Klein-Gordon equation. The Klein-Gordon equation for the EMS theory is given by

$$\frac{1}{\sqrt{-g}}\partial_\mu(\sqrt{-g}\partial^\mu\psi) = \frac{1}{4}\frac{df(\psi)}{d\psi}F_{\rho\sigma}F^{\rho\sigma}. \tag{B.10}$$

In this equation g is the determinant of the metric tensor. For the metric in Eq. (2.1.1) this determinant becomes

$$g = -A(r)B(r)r^4, \tag{B.11}$$

where we assumed spherical symmetry. Substituting the metric in the Klein-Gordon equation and rewriting the result gives

$$\psi''(r) = -\frac{f'(\psi)V'(r)^2}{2A(r)} - (\frac{2}{r} + \frac{A'(r)}{2A(r)} - \frac{B'(r)}{2B(r)})\psi'(r). \tag{B.12}$$

Varying the action with respect to the Maxwell invariant gives the equation

$$\partial_\mu(\sqrt{-g}f(\psi)F^{\mu\nu}) = 0. \tag{B.13}$$

Substituting the metric in this equation gives the Maxwell equation

$$V'(r) = \frac{\sqrt{A(r)B(r)}}{r^2 f(\psi)}Q. \tag{B.14}$$

Q is the charge of the modified black hole and is the integration constant that rises from Eq. (B.12). When we combine the Maxwell equation in Eq. (B.13), the Klein-Gordon equation in Eq. (B.11) and the results from the Einstein equation, we find the total

system of background equations

$$B'(r) = rB(r)\psi'(r)^2 + r\frac{B(r)}{A(r)}f(\psi)V'(r)^2 + \frac{B(r)}{r}(1 - B(r)), \tag{B.15a}$$

$$A'(r) = rA(r)\psi'(r)^2 + rf(\psi)V'(r)^2 + \frac{A(r)}{r}(B(r) - 1), \tag{B.15b}$$

$$V'(r) = \frac{\sqrt{A(r)B(r)}}{r^2 f(\psi)}Q, \tag{B.15c}$$

$$\psi''(r) = -\frac{f'(\psi)V'(r)^2}{2A(r)} - (\frac{2}{r} + \frac{A'(r)}{2A(r)} - \frac{B'(r)}{2B(r)})\psi'(r). \tag{B.15d}$$

B.2 Types of EMS black holes

To further specify the background solution in Eq. (B.15), it is necessary to choose a coupling function $f(\psi)$ and a potential $V(\psi)$. There are two subclasses of EMS black holes. Class I is called the dilatonic type. In this case the coupling function is given by

$$f(\psi) = e^{2\psi}. \tag{B.16}$$

In this case the $\psi = 0$ does not solve the background equation. That means that the Reissner-Nordström metric is not a solution of the background equations. However, in this case there will be a simple analytical solution to the background equation [19].

The EMS black hole case II type is the connected type. In this case, the derivative of the coupling function to ψ has to be zero for $\psi = 0$. For this case $\psi = 0$ does solve the background equation. As a consequence the Reissner-Nordström metric is a solution to the background equation. The black hole case II types can take different forms. Two of these forms are the scalarised-connected-type with

$$f(\psi) = e^{2\psi^2}, \tag{B.17}$$

and the scalarised-disconnected-type with

$$f(\psi) = 1 + \alpha\psi^4. \tag{B.18}$$

The background solution of case II type of EMS black holes has to be calculated numerically. The potential can be chosen to be a self-interacting scalar field or a free scalar field.

Free field:

$$V(\psi) = m^2\psi^2. \tag{B.19}$$

Self-interacting:

$$V(\psi) = m^2\psi^2 + \frac{\lambda}{2}\psi^4. \tag{B.20}$$

Now the background system can be solved for a certain coupling function and potential. The boundary conditions can be chosen near the event horizon or near infinity to the readers' own preference.